

Evolution of dark matter velocity dispersion

Alaric Erschfeld and Stefan Floerchinger

Institut für Theoretische Physik, Ruprecht-Karls-Universität Heidelberg,
Philosophenweg 16, D-69120 Heidelberg, Germany

E-mail: a.erschfeld@thphys.uni-heidelberg.de,
stefan.floerchinger@thphys.uni-heidelberg.de

Abstract. Cosmological perturbation theory for the late Universe dominated by dark matter is extended beyond the perfect fluid approximation by taking the dark matter velocity dispersion tensor as an additional field into account. A proper tensor decomposition of the latter leads to two additional scalar fields, as well as a vector and a tensor field. Most importantly, the trace of the velocity dispersion tensor can have a spatially homogeneous and isotropic expectation value. While it decays at early times, we show that a back-reaction effect quadratic in perturbations makes it grow strongly at late times. We compare sterile neutrinos as a candidate for comparatively warm dark matter to weakly interacting massive particles as a rather cold dark matter candidate and show that the late time growth of velocity dispersion is stronger for the latter. Another feature of a non-vanishing velocity dispersion expectation value is that it destroys the apparent self-consistency of the single-stream approximation and allows thereby to treat times and scales beyond shell-crossing.

Contents

1	Introduction	1
2	The Vlasov-Poisson system for dark matter	3
2.1	Dark matter distribution function, moments and cumulants	3
2.2	Statistical description and background-fluctuation splitting	5
2.3	Scalar, vector and tensor decomposition	6
2.4	Compact notation	10
3	Evolution of the background and linear fluctuations	12
3.1	Linear equations of motion	12
3.2	Scalar growth factors and free-streaming scale	14
3.3	Vector and tensor growth factors	16
3.4	Approximation for small velocity dispersion and soft power spectrum	18
4	Numerical results	21
4.1	Initial scalar power spectrum and velocity dispersion background	21
4.2	Results	23
5	Conclusion	30
A	Growth factors of the scalar and vector fields for negative $R(\eta)$	32

1 Introduction

The matter distribution throughout the Universe shows structures on a wide range of scales. Surveys indicate that matter is distributed homogeneous and isotropic on the largest scales, commonly referred to as the cosmological principle. But observations also show a rich variety of dense cosmological objects, from stars to galaxies, galaxy groups to galaxy clusters, forming filaments separated by immense voids making up the so-called cosmic web. It is assumed that these structures are the outcome of gravitational instabilities of near to scale-invariant and Gaussian initial density fluctuations in the matter distribution in an early epoch where the Universe is dominated by non-relativistic matter, dubbed *cold dark matter*. The collapse of matter is a competition between the expansion of the Universe and gravity, and current observations favour a scenario in which small scale structures collapse and virialise earlier than larger scale structures, also known as the bottom-up scenario [1, 2].

From a theoretical point of view, structure formation can be described by following the evolution of an ensemble of self-gravitating dark matter particles. Commonly this is done by considering Newtonian gravity because the scales under consideration are much smaller than the Hubble horizon, where general relativistic corrections need to be taken into account. One often uses a description in terms of classical kinetic theory for the phase-space distribution of dark matter particles. This uses the collisionless limit of the Boltzmann equation with gravitational fields, generically known as Vlasov equation. The further description is done in either of two frames. Eulerian coordinates are fixed to the expanding Friedmann-Lemaître-Robertson-Walker background cosmology, while Lagrangian coordinates follow the

trajectories of individual dark matter particles or the so-called displacement field [3]. Working in the former, one can consider *moments* or *cumulants* of the dark matter velocity distribution to obtain an infinite tower of coupled equations. Oftentimes they are truncated by setting the velocity dispersion tensor and higher cumulants to zero. The resulting equations describe dark matter as a perfect pressureless fluid. This is the so-called *single-stream approximation* since it assigns a unique velocity value to each point in space. Although the evolution equations are non-linear, these non-linearities are assumed to be small at early times and large scales and can therefore be treated perturbatively. For a review of standard cosmological perturbation theory we refer to reference [4].

Linear perturbation theory has had a tremendous success in describing the evolution of cosmic fields at early times and large scales. However, at later times and smaller scales, gravitational collapse becomes non-linear. A common way to deal with non-linearities in structure formation are numerical N -body simulations [5, 6]. While these allow to study structure formation in detail over a large amount of scales, they are limited by computational power. For this reason and to gain further insight into the mechanisms at play, different theoretical schemes have been put forward. Higher orders in perturbation theory have been calculated [7–12], various resummation schemes have been devised [13–35], effective field theory methods for a description of larger scales have been developed [36–55] and the renormalisation group for a (statistical) field theoretic description has been studied [56, 57].

However, to the extent that these methods are based on the single-stream approximation, they are ultimately limited to early times or very large scales. The approximation breaks down when multiple streams of matter coexist at the same region in space, a phenomenon known as *shell-crossing*. By definition, the single-stream approximation can not account for multiple velocities at the same point in space. In Lagrangian coordinates, the gravitational force becomes intrinsically non-local after stream crossing and thus the density field can no longer be approximated as an expansion of the determinant of the local deformation tensor.

There have been a number of works addressing this fundamental flaw in the description of dark matter. In an approach to estimate the effects of shell-crossing in Eulerian perturbation theory, reference [58] computed the back-reaction of vorticity and velocity dispersion generation on the density and velocity-divergence fields using numerical simulations. In references [59] and [60], velocity dispersion has been accounted for explicitly in the derivation from the Vlasov equation as source terms which are provided by numerical N -body simulations. Similarly, reference [40] formulated an effective field theory by extending Lagrangian perturbation theory with sources. These encode small scale effects such as shell-crossing and the long wavelength expansion is fitted using numerical simulations. All these approaches are in some way ‘effective’ in the sense that they encode the small scale effects in parameters which need to be fitted using numerical simulations. More recently, advances have been made in the Lagrangian picture in terms of 1+1 dimensional gravity, where Zel’dovich dynamics are exact up to shell-crossing [61–66]. Rather than pursuing down this road we extend the Eulerian framework similarly as has been started in reference [67].

Let us recall that the insufficiency of the single-stream approximation is due to the truncation of the infinite Vlasov hierarchy. The single-stream approximation seems to be self-consistent if velocity dispersion is absent, but is unstable under perturbations. Including the second cumulant of the velocity distribution, namely velocity dispersion, introduces new degrees of freedom which allow to account for multiple streams within the fluid description. While velocity dispersion effects should be relatively small for cold dark matter, their corrections are expected to kick in at small enough scales. As we show, even a small seed of velocity

dispersion can lead to accountable corrections at late times and small scales.

The other aspect we want to start investigating in this paper are cosmological vector and tensor fields. The single-stream approximation is described by two scalar fields, namely the density and velocity-divergence, while the only vector field present is the curl of the velocity field, the vorticity field. It is well known that at linear level the vorticity field decays due to the expansion of the Universe. In the single-stream approximation there are no non-linear terms which source vector fields from scalar initial conditions only. However, after including a non-vanishing velocity dispersion tensor we find that vector and tensor fields are non-linearly sourced by scalar fields. In the present paper we treat the full set of four scalar, two vector and one tensor matter degrees of freedom on linear level. In future follow-up work we plan to address non-linear dynamics in this setup.

2 The Vlasov-Poisson system for dark matter

2.1 Dark matter distribution function, moments and cumulants

We assume that dark matter consists of non-relativistic, classical point particles of mass m which interact only gravitationally, at least to leading approximation. We work in an approximation where the metric is in the conformal Newtonian gauge [68]

$$ds^2 = a^2(\tau) \left[- (1 + 2\phi(\tau, \mathbf{x})) d\tau^2 + (1 - 2\phi(\tau, \mathbf{x})) d\mathbf{x}^2 \right], \quad (2.1)$$

with the scale factor $a(\tau)$ and peculiar Newtonian gravitational potential $\phi(\tau, \mathbf{x})$. The conformal time τ is related to standard cosmic time t by $dt = a(\tau) d\tau$. The gravitational potential is assumed to be relatively small on the scales we are interested in and for $\phi(\tau, \mathbf{x}) = 0$ the space-time has the symmetries of a flat Friedmann-Lemaître-Robertson-Walker cosmology.¹ For a cosmology accounting for a cosmological constant and one dark matter species only, the evolution of the scale factor is determined by the Friedmann equations [69]

$$\frac{\dot{\mathcal{H}}(\tau)}{\mathcal{H}^2(\tau)} = 1 - \frac{3}{2} \Omega_m(\tau), \quad 1 = \Omega_m(\tau) + \Omega_\Lambda(\tau), \quad (2.2)$$

assuming dark matter to be pressureless at large enough scales. Here $\mathcal{H}(\tau) \equiv \dot{a}(\tau)/a(\tau)$ is the conformal Hubble parameter where we denote partial derivatives with respect to τ by a dot. Moreover, $\Omega_m(\tau)$ and $\Omega_\Lambda(\tau)$ are the dark matter and cosmological constant density parameters at τ , respectively. On scales much smaller than the Hubble horizon $1/\mathcal{H}(\tau)$, the gravitational potential is in first order approximation subject to Poisson's equation

$$\Delta_{\mathbf{x}}\phi = \frac{3}{2} \mathcal{H}^2 \Omega_m \delta, \quad (2.3)$$

where we suppress time and space arguments when unambiguous to simplify notation. The dark matter mass density fluctuation field $\delta(\tau, \mathbf{x})$ is defined below.

Dark matter is described in the framework of a kinetic theory approximation by the one-particle phase-space distribution function $f(\tau, \mathbf{x}, \mathbf{p})$ such that the number of particles in the comoving phase-space volume $d^3x d^3p$ at (\mathbf{x}, \mathbf{p}) and τ is

$$f(\tau, \mathbf{x}, \mathbf{p}) d^3x d^3p. \quad (2.4)$$

¹These symmetries actually become *statistical symmetries* for the full theory where the expectation values are either taken as spatial averages over large enough volumes or for conveniently defined ensembles of cosmologies.

Single dark matter particles move along the characteristics [70]

$$\frac{d\mathbf{x}}{d\tau} = \frac{\mathbf{p}}{a m}, \quad \frac{d\mathbf{p}}{d\tau} = -a m \nabla_{\mathbf{x}}\phi, \quad (2.5)$$

such that the dark matter distribution function is conserved along them. This leads to the Vlasov equation for the distribution function

$$\partial_{\tau}f + \frac{\mathbf{P}}{a m} \cdot \nabla_{\mathbf{x}}f - a m \nabla_{\mathbf{x}}\phi \cdot \nabla_{\mathbf{p}}f = 0. \quad (2.6)$$

To close the Vlasov-Poisson system of equations (2.3) and (2.6), we need the dark matter mass density field

$$\rho(\tau, \mathbf{x}) = \frac{m}{a^3(\tau)} \int_{\mathbb{R}^3} d^3p f(\tau, \mathbf{x}, \mathbf{p}). \quad (2.7)$$

It is convenient to split the density field into a spatially homogeneous expectation value

$$\bar{\rho}(\tau) \equiv \langle \rho(\tau, \mathbf{x}) \rangle, \quad (2.8)$$

which determines the density parameter $\Omega_m(\tau)$ and the locally varying dark matter mass density fluctuation field

$$\delta(\tau, \mathbf{x}) \equiv \frac{\rho(\tau, \mathbf{x}) - \bar{\rho}(\tau)}{\bar{\rho}(\tau)}. \quad (2.9)$$

Since the latter enters Poisson's equation (2.3), the Vlasov-Poisson system of equations is non-linear.

The Vlasov-Poisson system is closed and specifies the time evolution of the dark matter distribution function $f(\tau, \mathbf{x}, \mathbf{p})$ and the metric parametrised by the gravitational potential $\phi(\tau, \mathbf{x})$. A theoretical drawback when considering the distribution function is that it is a function of seven variables which makes it naturally difficult to solve the full Vlasov-Poisson system of equations. Also in a statistical description where one considers expectation values such as $\langle f(\tau, \mathbf{x}, \mathbf{p}) \rangle$ or correlation functions $\langle f(\tau, \mathbf{x}, \mathbf{p}) f(\tau', \mathbf{x}', \mathbf{p}') \rangle$, the symmetries reduce the complexity only little. On the other side, from an observational point of view, one is oftentimes not interested in the full phase-space distribution function but rather in *moments* with respect to the momentum argument. The zeroth moment is the dark matter mass density field (2.7). The first moment of the distribution function is given by the peculiar velocity field

$$u_i(\tau, \mathbf{x}) = \frac{1}{\rho(\tau, \mathbf{x})} \frac{m}{a(\tau)^3} \int_{\mathbb{R}^3} d^3p \frac{p_i}{a(\tau) m} f(\tau, \mathbf{x}, \mathbf{p}). \quad (2.10)$$

Similarly, the second moment can be parametrised by the peculiar velocity dispersion tensor field

$$\sigma_{ij}(\tau, \mathbf{x}) = \frac{1}{\rho(\tau, \mathbf{x})} \frac{m}{a(\tau)^3} \int_{\mathbb{R}^3} d^3p \frac{p_i p_j}{a(\tau)^2 m^2} f(\tau, \mathbf{x}, \mathbf{p}) - u_i(\tau, \mathbf{x}) u_j(\tau, \mathbf{x}), \quad (2.11)$$

which is the second *cumulant* and quantifies the deviation of particle velocities from the velocity field $u_i(\tau, \mathbf{x})$. Higher moments as well as cumulants of $f(\tau, \mathbf{x}, \mathbf{p})$ can be defined very similar to (2.10) and (2.11) in close analogy to the usual definitions for probability distributions.

By taking cumulants of the Vlasov equation (2.6) with respect to the momentum argument, one derives evolution equations for the corresponding matter fields. The expectation value of the zeroth moment yields

$$\dot{\bar{\rho}} + 3\mathcal{H}\bar{\rho} = 0, \quad (2.12)$$

and the local part can be reduced to the continuity equation

$$\dot{\delta} + u_i \delta_{,i} + (1 + \delta) u_{i,i} = 0 . \quad (2.13)$$

Similarly, the velocity field is subject to the Cauchy momentum equation

$$\dot{u}_i + \mathcal{H} u_i + u_j u_{i,j} + \sigma_{ij,j} + \sigma_{ij} \ln(1 + \delta)_{,j} + \phi_{,i} = 0 , \quad (2.14)$$

and the velocity dispersion tensor field obeys the velocity dispersion equation

$$\dot{\sigma}_{ij} + 2\mathcal{H} \sigma_{ij} + u_k \sigma_{ij,k} + \sigma_{jk} u_{i,k} + \sigma_{ik} u_{j,k} = -\pi_{ijk,k} - \pi_{ijk} \ln(1 + \delta)_{,k} , \quad (2.15)$$

where $\pi_{ijk}(\tau, \mathbf{x})$ is the third cumulant of the distribution function. We use a notation where a comma indicates partial derivatives with respect to the components of \mathbf{x} and we use the Einstein summation convention.

The so derived evolution equation for the n -th cumulant depends on the $(n + 1)$ -th cumulant creating an infinity hierarchy of coupled equations. To have a finite set of closed equations one needs to truncate the Vlasov hierarchy in an appropriate way. Often this is done by assuming dark matter to behave like a perfect pressureless fluid and setting $\sigma_{ij}(\tau, \mathbf{x}) \equiv 0$, the so-called *single-stream approximation*. By definition the single-stream approximation can not account for multiple streams within the fluid and therefore can not describe the phenomenon of *shell-crossing*, when trajectories of particles meet in configuration space. In order to overcome this deficit we truncate the Vlasov hierarchy at the next higher cumulant, thereby accounting for velocity dispersion within the fluid description. A priori it is not self-consistent to neglect all higher cumulants, since these are sourced by terms which solely depend on the lower cumulants [58].² However, *cum grano salis* we assume this truncation to be appropriate for cosmological scales and dark matter with sufficient small velocity dispersion and henceforth set $\pi_{ijk}(\tau, \mathbf{x}) \equiv 0$.

2.2 Statistical description and background-fluctuation splitting

We are interested in a statistical description of dark matter formulated in terms of expectation values and correlation functions of the cosmological fields. The latter are given by the gravitational potential $\phi(\tau, \mathbf{x})$ as well as the matter fields defined by the zeroth momentum-momentum (2.7) and the first two momentum-cumulants (2.10) and (2.11) of the dark matter distribution function $f(\tau, \mathbf{x}, \mathbf{p})$.

The statistical field theory we employ can be seen as describing an ensemble of cosmological histories with stochastic initial conditions or, equivalently for this purpose, an ensemble of different spatial subvolumes of a single cosmological history. We assume that the symmetries of the idealised flat Friedmann-Lemaître-Robertson-Walker cosmology are realised as statistical symmetries for this field theory which concerns in particular spatial translations and rotations.

In the following it is convenient to split the cosmological fields into a background and a fluctuation part. The background is taken to be spatially homogeneous and isotropic and corresponds to the expectation value of the fields. For the density field we have already done such a splitting in the definitions (2.8) and (2.9). For the velocity field $u_i(\tau, \mathbf{x})$ the statistical

²In contrast, truncating the Vlasov hierarchy in the single-stream approximation seems to be superficially self-consistent since there are no source terms in the equations of motion of higher cumulants which solely depend on the density fluctuation field $\delta(\tau, \mathbf{x})$ and/or the velocity field $u_i(\tau, \mathbf{x})$.

rotation symmetry forbids an expectation value such that it is a pure fluctuation field. For the velocity dispersion tensor field defined in (2.11) one may have a non-vanishing isotropic expectation value,

$$\langle \sigma_{ij}(\tau, \mathbf{x}) \rangle = \delta_{ij} \bar{\sigma}(\tau). \quad (2.16)$$

Note that $\bar{\sigma}(\tau)$ is positive semi-definite and in the following we assume $\bar{\sigma}(\tau) > 0$, although the value could be very small. Similar to the density fluctuation field (2.9) we define the peculiar velocity dispersion tensor fluctuation field

$$\varsigma_{ij}(\tau, \mathbf{x}) \equiv \frac{\sigma_{ij}(\tau, \mathbf{x}) - \delta_{ij} \bar{\sigma}(\tau)}{\bar{\sigma}(\tau)}. \quad (2.17)$$

The velocity dispersion background $\bar{\sigma}(\tau)$ obeys the expectation value of the trace of the velocity dispersion equation (2.15), given by

$$\dot{\bar{\sigma}}(\tau) + \left[2\mathcal{H}(\tau) + \frac{1}{3} \langle \varsigma_{ii,j}(\tau, \mathbf{x}) u_j(\tau, \mathbf{x}) \rangle + \frac{2}{3} \langle \varsigma_{ij}(\tau, \mathbf{x}) u_{i,j}(\tau, \mathbf{x}) \rangle \right] \bar{\sigma}(\tau) = 0. \quad (2.18)$$

In contrast to the evolution equation of the density background (2.12) the evolution of the velocity dispersion background depends on equal-time two-point correlation functions of the velocity and the velocity dispersion fluctuation fields.

Note that the expectation value (2.16) differs from a possible expectation value of the pressure of the dark matter fluid which would instead be given by

$$\langle \rho(\tau, \mathbf{x}) \sigma_{ij}(\tau, \mathbf{x}) \rangle = \delta_{ij} \bar{P}(\tau). \quad (2.19)$$

In terms of the background-fluctuation splitting (2.16) and (2.17), the Cauchy momentum equation (2.14) and velocity dispersion equation (2.15) can be written as

$$\dot{u}_i + \mathcal{H} u_i + u_j u_{i,j} + \bar{\sigma} \varsigma_{ij,j} + \bar{\sigma} \ln(1 + \delta)_{,i} + \bar{\sigma} \varsigma_{ij} \ln(1 + \delta)_{,j} + \phi_{,i} = 0, \quad (2.20)$$

and

$$\dot{\varsigma}_{ij} + \left(2\mathcal{H} + \frac{\dot{\bar{\sigma}}}{\bar{\sigma}} \right) \varsigma_{ij} + u_{i,j} + u_{j,i} + u_k \varsigma_{ij,k} + \varsigma_{jk} u_{i,k} + \varsigma_{ik} u_{j,k} + \delta_{ij} \left(2\mathcal{H} + \frac{\dot{\bar{\sigma}}}{\bar{\sigma}} \right) = 0. \quad (2.21)$$

The last term on the left side of equation (2.21) is a background term which, together with the evolution equation (2.18), ensures that $\langle \dot{\varsigma}_{ij}(\tau, \mathbf{x}) \rangle = 0$. Note that $\bar{\sigma}(\tau)$ enters the equations of motion (2.20) and (2.21) and that the evolution equation (2.18) depends on the two-point correlation function of the fluctuation fields. In this sense, the background and fluctuation fields are coupled and need to be solved simultaneously.

2.3 Scalar, vector and tensor decomposition

For further analysis we decompose the matter fields according to their transformation properties under spatial rotations into scalar, vector and tensor fields. This is most conveniently done by moving to Fourier space using the convention

$$f(\mathbf{k}) \equiv \int_{\mathbf{x}} e^{-i\mathbf{k}\cdot\mathbf{x}} f(\mathbf{x}), \quad f(\mathbf{x}) \equiv \int_{\mathbf{k}} e^{i\mathbf{k}\cdot\mathbf{x}} f(\mathbf{k}), \quad (2.22)$$

for any integrable field $f(\mathbf{x})$ where we abbreviate configuration and Fourier space integrals by

$$\int_{\mathbf{x}} \equiv \int_{\mathbb{R}^3} d^3x, \quad \int_{\mathbf{k}} \equiv \int_{\mathbb{R}^3} \frac{d^3k}{(2\pi)^3}. \quad (2.23)$$

The velocity fluctuation field $u_i(\tau, \mathbf{k})$ can be decomposed into an irrotational and a solenoidal vector field. The irrotational part of the decomposition can be parametrised in terms of the scalar peculiar velocity-divergence field

$$\theta(\tau, \mathbf{k}) \equiv ik_j u_j(\tau, \mathbf{k}), \quad (2.24)$$

and describes the potential flow of the dark matter fluid. The remaining solenoidal part can be parametrised by the peculiar vorticity field

$$\omega_j(\tau, \mathbf{k}) \equiv \varepsilon_{jkl} ik_k u_l(\tau, \mathbf{k}), \quad (2.25)$$

which quantifies the local rotation of fluid elements. The vorticity field $\omega_i(\tau, \mathbf{k})$ is a pseudovector field which is transverse to the flow direction \mathbf{k} . In terms of the velocity-divergence and vorticity fields, the decomposition takes the form

$$u_j(\tau, \mathbf{k}) = -\frac{ik_j}{k^2} \theta(\tau, \mathbf{k}) + \varepsilon_{jkl} \frac{ik_k}{k^2} \omega_l(\tau, \mathbf{k}). \quad (2.26)$$

Similarly, the symmetric second-rank velocity dispersion tensor fluctuation field $\varsigma_{ij}(\tau, \mathbf{k})$ can be decomposed into two scalar fields, a solenoidal vector field and a symmetric, transverse and traceless second-rank tensor field [71]. We parametrise the scalar fields in terms of the trace field

$$\varsigma(\tau, \mathbf{k}) \equiv \frac{\delta_{ij}}{3} \varsigma_{ij}(\tau, \mathbf{k}), \quad (2.27)$$

and the off-trace field

$$\vartheta(\tau, \mathbf{k}) \equiv \left(\frac{k_i k_j}{k^2} - \frac{\delta_{ij}}{3} \right) \varsigma_{ij}(\tau, \mathbf{k}), \quad (2.28)$$

which quantify isotropic and anisotropic velocity dispersion, respectively. The solenoidal vector field we parametrise by

$$\vartheta_i(\tau, \mathbf{k}) \equiv \varepsilon_{ijk} \frac{k_j k_l}{k^2} \varsigma_{kl}(\tau, \mathbf{k}), \quad (2.29)$$

and the symmetric, transverse and traceless second-rank tensor field by

$$\vartheta_{ij}(\tau, \mathbf{k}) \equiv \Delta_{ijkl}(\mathbf{k}) \varsigma_{kl}(\tau, \mathbf{k}), \quad (2.30)$$

both of which describe anisotropic velocity dispersion degrees of freedom. Here we introduced the symmetric, transverse and traceless projector

$$\Delta_{ijkl}(\mathbf{k}) \equiv \frac{1}{2} \left[\Delta_{ik}(\mathbf{k}) \Delta_{jl}(\mathbf{k}) + \Delta_{il}(\mathbf{k}) \Delta_{jk}(\mathbf{k}) - \Delta_{ij}(\mathbf{k}) \Delta_{kl}(\mathbf{k}) \right], \quad (2.31)$$

defined in terms of the transverse projector

$$\Delta_{ij}(\mathbf{k}) \equiv \delta_{ij} - \frac{k_i k_j}{k^2}. \quad (2.32)$$

The decomposition of the velocity dispersion tensor fluctuation field $\varsigma_{ij}(\tau, \mathbf{k})$ can then be written as

$$\begin{aligned} \varsigma_{ij}(\tau, \mathbf{k}) = & \delta_{ij} \varsigma(\tau, \mathbf{k}) + \frac{3}{2} \left(\frac{k_i k_j}{k^2} - \frac{\delta_{ij}}{3} \right) \vartheta(\tau, \mathbf{k}) - \frac{(\varepsilon_{ikl} k_j + \varepsilon_{jkl} k_i) k_k}{k^2} \vartheta_l(\tau, \mathbf{k}) \\ & + \Delta_{ijkl}(\mathbf{k}) \vartheta_{kl}(\tau, \mathbf{k}) . \end{aligned} \quad (2.33)$$

All ten matter degrees of freedom are described by the four scalar fields $(\delta, \theta, \varsigma, \vartheta)$, the two solenoidal vector fields (ω_i, ϑ_i) and the symmetric, transverse and traceless second-rank tensor field ϑ_{ij} .

In order to rewrite the background evolution equation (2.18) in terms of expectation values of the decomposed fluctuation fields it is convenient to define the equal-time power spectra

$$\begin{aligned} (2\pi)^3 \delta_D^{(3)}(\mathbf{k} + \mathbf{k}') P_{\varsigma\theta}(\tau, k) & \equiv \langle \varsigma(\tau, \mathbf{k}) \theta(\tau, \mathbf{k}') \rangle , \\ (2\pi)^3 \delta_D^{(3)}(\mathbf{k} + \mathbf{k}') P_{\vartheta\theta}(\tau, k) & \equiv \langle \vartheta(\tau, \mathbf{k}) \theta(\tau, \mathbf{k}') \rangle , \\ (2\pi)^3 \delta_D^{(3)}(\mathbf{k} + \mathbf{k}') \Delta_{ij}(\mathbf{k}) P_{\vartheta\omega}(\tau, k) & \equiv \langle \vartheta_i(\tau, \mathbf{k}) \omega_j(\tau, \mathbf{k}') \rangle , \end{aligned} \quad (2.34)$$

and the dimensionless function

$$Q(\tau) \equiv \frac{1}{3} \int_{\mathbf{q}} \left[P_{\varsigma\theta}(\tau, q) - 2 P_{\vartheta\theta}(\tau, q) - 4 P_{\vartheta\omega}(\tau, q) \right] , \quad (2.35)$$

where $\delta_D^{(n)}(x)$ is the Dirac delta function in n dimensions. The background evolution equation (2.18) can then be rewritten to

$$\dot{\bar{\sigma}}(\tau) + \left(2\mathcal{H}(\tau) - Q(\tau) \right) \bar{\sigma}(\tau) = 0 . \quad (2.36)$$

With equation (2.36) it is evident that the function $Q(\tau)$ quantifies the dependence of the velocity dispersion background on the decomposed fluctuation fields.

To cast the left side of the Cauchy momentum equation (2.20) into a form which is a polynomial of finite degree in the decomposed fluctuation fields, we Taylor expand the logarithmic density field $\ln(1 + \delta(\tau, \mathbf{x}))$ around the background configuration $\delta(\tau, \mathbf{x}) = 0$ up to third order in $\delta(\tau, \mathbf{x})$ and neglect all higher terms.³ By splitting the equations of motion (2.13), (2.20) and (2.21) for $\mathbf{k} \neq 0$ according to the decompositions (2.26) and (2.33) and using Poisson's equation (2.3) as well as the background evolution equation (2.36) one is left with the continuity equation

$$\dot{\delta} + \theta + I_\delta = 0 , \quad (2.37)$$

the velocity-divergence equation

$$\dot{\theta} + \mathcal{H}\theta - k^2 \bar{\sigma} (\varsigma + \vartheta) + \left(\frac{3}{2} \mathcal{H}^2 \Omega_m - k^2 \bar{\sigma} \right) \delta + I_\theta + J_\theta = 0 , \quad (2.38)$$

the vorticity equation

$$\dot{\omega}_i + \mathcal{H}\omega_i - k^2 \bar{\sigma} \vartheta_i + I_\omega^i + J_\omega^i = 0 , \quad (2.39)$$

³Higher order terms in the fluctuation fields do not enter one-loop calculations within the framework of renormalised cosmological perturbation theory [14].

and the four velocity dispersion equations

$$\dot{\zeta} + Q \zeta + \frac{2}{3} \theta + I_\zeta = 0, \quad (2.40)$$

$$\dot{\vartheta} + Q \vartheta + \frac{4}{3} \theta + I_\vartheta = 0, \quad (2.41)$$

$$\dot{\vartheta}_i + Q \vartheta_i + \omega_i + I_\vartheta^i = 0, \quad (2.42)$$

$$\dot{\vartheta}_{ij} + Q \vartheta_{ij} + I_\vartheta^{ij} = 0. \quad (2.43)$$

To parametrise the terms quadratic in the decomposed fluctuation fields we introduced for the continuity equation (2.37) the abbreviation

$$I_\delta(\tau, \mathbf{k}) \equiv \int_{\mathbf{k}_1, \mathbf{k}_2} \left[A_{\theta\delta} \theta_1 \delta_2 + A_{\omega\delta}^i \omega_{i1} \delta_2 \right]. \quad (2.44)$$

Similarly, for the velocity-divergence and vorticity equations (2.38) and (2.39) we abbreviate

$$\begin{aligned} I_\theta(\tau, \mathbf{k}) &\equiv \int_{\mathbf{k}_1, \mathbf{k}_2} \left[B_{\theta\theta} \theta_1 \theta_2 + B_{\theta\omega}^i \theta_1 \omega_{i2} + B_{\omega\omega}^{ij} \omega_{i1} \omega_{j2} + k^2 \bar{\sigma} B_{\delta\delta} \delta_1 \delta_2 \right. \\ &\quad \left. + k^2 \bar{\sigma} B_{\zeta\delta} \zeta_1 \delta_2 + k^2 \bar{\sigma} B_{\vartheta\delta} \vartheta_1 \delta_2 + k^2 \bar{\sigma} B_{\vartheta\delta}^i \vartheta_{i1} \delta_2 + k^2 \bar{\sigma} B_{\vartheta\delta}^{ij} \vartheta_{ij1} \delta_2 \right], \\ I_\omega^i(\tau, \mathbf{k}) &\equiv \int_{\mathbf{k}_1, \mathbf{k}_2} \left[C_{\theta\omega}^{ij} \theta_1 \omega_{j2} + C_{\omega\omega}^{ijk} \omega_{j1} \omega_{k2} + k^2 \bar{\sigma} C_{\zeta\delta}^i \zeta_1 \delta_2 \right. \\ &\quad \left. + k^2 \bar{\sigma} C_{\vartheta\delta}^i \vartheta_1 \delta_2 + k^2 \bar{\sigma} C_{\vartheta\delta}^{ij} \vartheta_{j1} \delta_2 + k^2 \bar{\sigma} C_{\vartheta\delta}^{ijk} \vartheta_{jk1} \delta_2 \right], \end{aligned} \quad (2.45)$$

and in the velocity dispersion equations (2.40) – (2.43) we use

$$\begin{aligned} I_\zeta(\tau, \mathbf{k}) &\equiv \int_{\mathbf{k}_1, \mathbf{k}_2} \left[D_{\zeta\theta} \zeta_1 \theta_2 + D_{\zeta\omega}^i \zeta_1 \omega_{i2} + D_{\vartheta\theta} \vartheta_1 \theta_2 + D_{\vartheta\omega}^i \vartheta_1 \omega_{i2} \right. \\ &\quad \left. + D_{\vartheta\theta}^i \vartheta_{i1} \theta_2 + D_{\vartheta\omega}^{ij} \vartheta_{i1} \omega_{j2} + D_{\vartheta\theta}^{ij} \vartheta_{ij1} \theta_2 + D_{\vartheta\omega}^{ijk} \vartheta_{ij1} \omega_{k2} \right], \\ I_\vartheta(\tau, \mathbf{k}) &\equiv \int_{\mathbf{k}_1, \mathbf{k}_2} \left[E_{\zeta\theta} \zeta_1 \theta_2 + E_{\zeta\omega}^i \zeta_1 \omega_{i2} + E_{\vartheta\theta} \vartheta_1 \theta_2 + E_{\vartheta\omega}^i \vartheta_1 \omega_{i2} \right. \\ &\quad \left. + E_{\vartheta\theta}^i \vartheta_{i1} \theta_2 + E_{\vartheta\omega}^{ij} \vartheta_{i1} \omega_{j2} + E_{\vartheta\theta}^{ij} \vartheta_{ij1} \theta_2 + E_{\vartheta\omega}^{ijk} \vartheta_{ij1} \omega_{k2} \right], \\ I_\vartheta^i(\tau, \mathbf{k}) &\equiv \int_{\mathbf{k}_1, \mathbf{k}_2} \left[F_{\zeta\theta}^i \zeta_1 \theta_2 + F_{\zeta\omega}^{ij} \zeta_1 \omega_{j2} + F_{\vartheta\theta}^i \vartheta_1 \theta_2 + F_{\vartheta\omega}^{ij} \vartheta_1 \omega_{j2} \right. \\ &\quad \left. + F_{\vartheta\theta}^{ij} \vartheta_{j1} \theta_2 + F_{\vartheta\omega}^{ijk} \vartheta_{j1} \omega_{k2} + F_{\vartheta\theta}^{ijk} \vartheta_{jk1} \theta_2 + F_{\vartheta\omega}^{ijkl} \vartheta_{jk1} \omega_{l2} \right], \\ I_\vartheta^{ij}(\tau, \mathbf{k}) &\equiv \int_{\mathbf{k}_1, \mathbf{k}_2} \left[G_{\zeta\theta}^{ij} \zeta_1 \theta_2 + G_{\zeta\omega}^{ijk} \zeta_1 \omega_{k2} + G_{\vartheta\theta}^{ij} \vartheta_1 \theta_2 + G_{\vartheta\omega}^{ijk} \vartheta_1 \omega_{k2} \right. \\ &\quad \left. + G_{\vartheta\theta}^{ijk} \vartheta_{k1} \theta_2 + G_{\vartheta\omega}^{ijkl} \vartheta_{k1} \omega_{l2} + G_{\vartheta\theta}^{ijkl} \vartheta_{kl1} \theta_2 + G_{\vartheta\omega}^{ijklm} \vartheta_{kl1} \omega_{m2} \right]. \end{aligned} \quad (2.46)$$

Finally, the terms cubic in the decomposed fluctuation fields are abbreviated as

$$\begin{aligned}
J_\theta(\tau, \mathbf{k}) &\equiv \int_{\mathbf{k}_1, \mathbf{k}_2, \mathbf{k}_3} k^2 \bar{\sigma} \left[B_{\delta\delta\delta} \delta_1 \delta_2 \delta_3 + B_{\varsigma\delta\delta} \varsigma_1 \delta_2 \delta_3 \right. \\
&\quad \left. + B_{\vartheta\delta\delta} \vartheta_1 \delta_2 \delta_3 + B_{\vartheta\delta\delta}^i \vartheta_{i1} \delta_2 \delta_3 + B_{\vartheta\delta\delta}^{ij} \vartheta_{ij1} \delta_2 \delta_3 \right], \quad (2.47) \\
J_\omega^i(\tau, \mathbf{k}) &\equiv \int_{\mathbf{k}_1, \mathbf{k}_2, \mathbf{k}_3} k^2 \bar{\sigma} \left[C_{\varsigma\delta\delta}^i \varsigma_1 \delta_2 \delta_3 + C_{\vartheta\delta\delta}^i \vartheta_1 \delta_2 \delta_3 + C_{\vartheta\delta\delta}^{ij} \vartheta_{j1} \delta_2 \delta_3 + C_{\vartheta\delta\delta}^{ijk} \vartheta_{jk1} \delta_2 \delta_3 \right].
\end{aligned}$$

All fields are evaluated at τ and in order to simplify notation we denoted a field with the wave vector argument \mathbf{k}_1 , \mathbf{k}_2 or \mathbf{k}_3 by a subscripted 1, 2 or 3, respectively. The vertices A, B, C, D, E, F and G are the convolution kernels of the Fourier transformation of the terms non-linear in the decomposed fluctuation fields. They carry an overall momentum conserving Dirac delta function and depend on the wave vectors which are integrated over. We provide the explicit form of these vertices in a future publication.

Note that the assumption of a non-vanishing $\bar{\sigma}(\tau)$ breaks the apparent self-consistency of the single-stream approximation since the scalar and vector velocity dispersion fields are sourced at linear level by the scalar and vector velocity fields, respectively. Further, the velocity dispersion background enters the velocity fluctuation field equations (2.38) and (2.39) in the combination $k^2 \bar{\sigma}(\tau)$, as is required by dimensional arguments. This introduces a scale dependence even at linear order in the decomposed fluctuation fields which is essential for the convergence of the linear theory.

Because the single-stream approximation features only the vertices $C_{\theta\omega}^{ij}(\mathbf{k}_1, \mathbf{k}_2)$ and $C_{\omega\omega}^{ijk}(\mathbf{k}_1, \mathbf{k}_2)$ for the generation of the vorticity field, it is not possible to excite vector fields from scalar initial conditions. In contrast, by including velocity dispersion, it is possible to source vector and tensor fields non-linearly from scalar initial conditions only through the vertices $C_{\varsigma\delta}^i(\mathbf{k}_1, \mathbf{k}_2)$, $C_{\vartheta\delta}^i(\mathbf{k}_1, \mathbf{k}_2)$, $C_{\varsigma\delta\delta}^i(\mathbf{k}_1, \mathbf{k}_2, \mathbf{k}_3)$, $C_{\vartheta\delta\delta}^i(\mathbf{k}_1, \mathbf{k}_2, \mathbf{k}_3)$, $F_{\varsigma\theta}^i(\mathbf{k}_1, \mathbf{k}_2)$, $F_{\vartheta\theta}^i(\mathbf{k}_1, \mathbf{k}_2)$, $G_{\varsigma\theta}^{ij}(\mathbf{k}_1, \mathbf{k}_2)$, $G_{\vartheta\theta}^{ij}(\mathbf{k}_1, \mathbf{k}_2)$, provided a non-vanishing velocity dispersion background.

2.4 Compact notation

To cast the equations of motion (2.37) – (2.43) into a more symmetric and compact form we introduce the time evolution parameter

$$\eta(\tau) \equiv \ln \left(\frac{D_+(\tau)}{D_+(\tau_{\text{in}})} \right), \quad (2.48)$$

corresponding to the number of e -folds of the linear growth function in the single-stream approximation [72]

$$D_+(\tau) = a(\tau) {}_2F_1 \left(\frac{1}{3}, 1; \frac{11}{6}; -a^3(\tau) \frac{1 - \Omega_{m,0}}{\Omega_{m,0}} \right), \quad (2.49)$$

normalised to unity at some initial time τ_{in} .⁴ Here the growth function is given in terms of the Gaussian hypergeometric function ${}_2F_1(a, b; c; x)$ and the dark matter density parameter is

⁴We assume a cosmology with a cosmological constant and one sufficiently cold dark matter species without radiative component.

written as $\Omega_m(\tau) = \Omega_{m,0}/a^3(\tau)$ where $\Omega_{m,0}$ is the value at $a(0) = 1$, corresponding to today. Further it is useful to define the function

$$f(\tau) \equiv \frac{\partial \ln(D_+(\tau))}{\partial \ln(a(\tau))} , \quad (2.50)$$

which parametrises the logarithmic deviation of $D_+(\tau)$ from the Einstein-de Sitter linear growth function $a(\tau)$ and obeys the evolution equation [59]

$$\partial_\eta \ln(f \mathcal{H}) = \frac{3}{2} \frac{\Omega_m}{f^2} - \frac{1}{f} - 1 . \quad (2.51)$$

In the following we use $\eta(\tau)$ rather than τ which are related through the definition (2.48).

Grouping scalar, vector and tensor fields in a condensed notation, we define the field vector

$$\Psi(\eta, \mathbf{k}) \equiv \begin{pmatrix} \delta(\eta, \mathbf{k}) \\ -\theta(\eta, \mathbf{k}) / (f(\eta) \mathcal{H}(\eta)) \\ \varsigma(\eta, \mathbf{k}) \\ \vartheta(\eta, \mathbf{k}) \\ \omega_i(\eta, \mathbf{k}) / (f(\eta) \mathcal{H}(\eta)) \\ \vartheta_i(\eta, \mathbf{k}) \\ \vartheta_{ij}(\eta, \mathbf{k}) \end{pmatrix} . \quad (2.52)$$

The component fields are referred to by $\Psi_a(\eta, \mathbf{k})$ where the index a runs over all fields and implicitly carries possible spatial indices which are only displayed if necessary. We use the Einstein summation convention which implies summation over possible carried vector or tensor indices. Scalar, vector and tensor fields are referred to by the indices a_s , a_v and a_t which run over the scalar, vector and tensor field components only. Similar to before we define the equal-time power spectra

$$(2\pi)^3 \delta_D^{(3)}(\mathbf{k} + \mathbf{k}') P_{ab}(\eta, k) \equiv \langle \Psi_a(\eta, \mathbf{k}) \Psi_b(\eta, \mathbf{k}') \rangle , \quad (2.53)$$

which depend only on the wave number k due to the statistical homogeneity and isotropy symmetry. The power spectrum (2.53) is naturally block diagonal for scalar, vector and tensor fields and is understood to implicitly carry a possible projector for the vector and tensor fields, i.e.

$$\begin{aligned} (2\pi)^3 \delta_D^{(3)}(\mathbf{k} + \mathbf{k}') \Delta_{ij}(\mathbf{k}) P_{a_v b_v}(\eta, k) &= \langle \Psi_{a_v}^i(\eta, \mathbf{k}) \Psi_{b_v}^j(\eta, \mathbf{k}') \rangle , \\ (2\pi)^3 \delta_D^{(3)}(\mathbf{k} + \mathbf{k}') \Delta_{ijkl}(\mathbf{k}) P_{a_t b_t}(\eta, k) &= \langle \Psi_{a_t}^{ij}(\eta, \mathbf{k}) \Psi_{b_t}^{kl}(\eta, \mathbf{k}') \rangle . \end{aligned} \quad (2.54)$$

It is convenient to also define the rescaled background

$$\hat{\sigma}(\eta) \equiv \frac{\bar{\sigma}(\eta)}{f^2(\eta) \mathcal{H}^2(\eta)} , \quad (2.55)$$

and introduce the dimensionless function

$$R(\eta) \equiv \frac{1}{3} \int_{\mathbf{q}} \left[-P_{32}(\eta, q) + 2P_{42}(\eta, q) - 4P_{65}(\eta, q) \right] , \quad (2.56)$$

such that the background evolution equation (2.36) can be written as

$$\partial_\eta \hat{\sigma}(\eta) + \left(3 \frac{\Omega_m(\eta)}{f^2(\eta)} - 2 - R(\eta) \right) \hat{\sigma}(\eta) = 0 . \quad (2.57)$$

Here $R(\eta)$ plays the same role for $\hat{\sigma}(\eta)$ as the function $Q(\tau)$ for $\bar{\sigma}(\tau)$. The equations of motion (2.37) – (2.43) can be cast into the form

$$\partial_\eta \Psi_a(\eta, \mathbf{k}) + \Omega_{ab}(\eta, k) \Psi_b(\eta, \mathbf{k}) + I_a(\eta, \mathbf{k}) + J_a(\eta, \mathbf{k}) = 0 , \quad (2.58)$$

where the coefficients of the terms linear in the decomposed fluctuation fields are given by the matrix $\Omega_{ab}(\eta, k)$. It is block diagonal for scalar, vector and tensor fields with the scalar submatrix

$$\Omega_{a_s b_s}(\eta, k) = \begin{pmatrix} 0 & -1 & 0 & 0 \\ -\frac{3}{2} \frac{\Omega_m(\eta)}{f^2(\eta)} + k^2 \hat{\sigma}(\eta) & \frac{3}{2} \frac{\Omega_m(\eta)}{f^2(\eta)} - 1 & k^2 \hat{\sigma}(\eta) & k^2 \hat{\sigma}(\eta) \\ 0 & -\frac{2}{3} & R(\eta) & 0 \\ 0 & -\frac{4}{3} & 0 & R(\eta) \end{pmatrix} , \quad (2.59)$$

and the vector and tensor submatrices

$$\Omega_{a_v b_v}(\eta, k) = \begin{pmatrix} \frac{3}{2} \frac{\Omega_m(\eta)}{f^2(\eta)} - 1 & -k^2 \hat{\sigma}(\eta) \\ 1 & R(\eta) \end{pmatrix} , \quad \Omega_{a_t b_t}(\eta, k) = R(\eta) . \quad (2.60)$$

Similar to the power spectra (2.54) they carry a vector or tensor projector, respectively. The non-linear terms quadratic in the decomposed fluctuation fields are given by

$$I_a(\eta, \mathbf{k}) = \int_{\mathbf{k}_1, \mathbf{k}_2} \delta_D^{(3)}(\mathbf{k} - \mathbf{k}_1 - \mathbf{k}_2) Y_{abc}(\eta, \mathbf{k}, \mathbf{k}_1, \mathbf{k}_2) \Psi_b(\eta, \mathbf{k}_1) \Psi_c(\eta, \mathbf{k}_2) , \quad (2.61)$$

whereas the terms cubic in the decomposed fluctuation fields are

$$J_a(\eta, \mathbf{k}) = \int_{\mathbf{k}_1, \mathbf{k}_2, \mathbf{k}_3} \delta_D^{(3)}(\mathbf{k} - \mathbf{k}_1 - \mathbf{k}_2 - \mathbf{k}_3) X_{abcd}(\eta, \mathbf{k}, \mathbf{k}_1, \mathbf{k}_2, \mathbf{k}_3) \times \Psi_b(\eta, \mathbf{k}_1) \Psi_c(\eta, \mathbf{k}_2) \Psi_d(\eta, \mathbf{k}_3) . \quad (2.62)$$

Here $Y_{abc}(\eta, \mathbf{k}, \mathbf{k}_1, \mathbf{k}_2)$ and $X_{abcd}(\eta, \mathbf{k}, \mathbf{k}_1, \mathbf{k}_2, \mathbf{k}_3)$ are symmetrised versions of the vertices appearing in equations (2.44) – (2.47).

3 Evolution of the background and linear fluctuations

3.1 Linear equations of motion

At early times and large scales we assume the fields $\Psi_a(\eta, \mathbf{k})$ to be small compared to the homogeneous and isotropic background. Therefore, it seems natural to study how the fields evolve in the linear regime where we neglect the coupling of different Fourier modes. In the limit where we turn off interactions, the equations of motion (2.58) reduce to

$$\partial_\eta \Psi_a(\eta, \mathbf{k}) + \Omega_{ab}(\eta, k) \Psi_b(\eta, \mathbf{k}) = 0 . \quad (3.1)$$

While the equations of motion (3.1) describe linear fields, in the sense that no interaction between Fourier modes is taken into account, they nevertheless form a set of non-linear differential equations because $R(\eta)$ implicitly depends on the power spectra of the fields. Additionally, the background evolution equation (2.57) is needed to close the system of equations because $\hat{\sigma}(\eta)$ enters $\Omega_{ab}(\eta, k)$. In this situation one cannot expect to find solutions in a closed form in terms of standard mathematical functions.

To fully determine the system we need to specify initial conditions at some initial time evolution parameter $\eta_{\text{in}} \equiv \eta(\tau_{\text{in}})$.⁵ In the following we use the approximation $\Omega_m(\tau)/f^2(\tau) = 1$, which is sufficiently accurate for the times we are interested in [73]. With an initial velocity dispersion background $\hat{\sigma}_{\text{in}}$, the background evolution equation (2.57) can be formally solved with

$$\hat{\sigma}(\eta) = \hat{\sigma}_{\text{in}} \exp \left\{ \int_{\eta_{\text{in}}}^{\eta} d\xi (R(\xi) - 1) \right\}. \quad (3.2)$$

Concerning the fields $\Psi_a(\eta, \mathbf{k})$, we assume that vector and tensor fields can be initially neglected and that the initial scalar fields can be written as proportional random fields,

$$\Phi_{a_s}(\mathbf{k}) = w_{a_s}(k) \delta^{\text{in}}(\mathbf{k}), \quad (3.3)$$

where $\delta^{\text{in}}(\mathbf{k})$ is the initial dark matter mass density fluctuation field. The vector $w_{a_s}(k)$ quantifies the proportionality of the initial conditions to $\delta^{\text{in}}(\mathbf{k})$ and we chose it to be the eigenvector of the growing solution as discussed below. The initial density fluctuation field $\delta^{\text{in}}(\mathbf{k})$ is assumed to be a Gaussian random field and therefore completely characterised by the initial scalar power spectrum

$$(2\pi)^3 P_s^{\text{in}}(k) \delta_{\text{D}}^{(3)}(\mathbf{k} + \mathbf{k}') \equiv \langle \delta_{\text{in}}(\mathbf{k}) \delta_{\text{in}}(\mathbf{k}') \rangle. \quad (3.4)$$

The fields $\Psi_a(\eta, \mathbf{k})$ can formally be written as the linear response to the initial conditions $\Phi_a(\mathbf{k})$,

$$\Psi_a(\eta, \mathbf{k}) = g_{ab}^R(\eta, \eta_{\text{in}}, k) \Phi_b(\mathbf{k}). \quad (3.5)$$

The Green's function $g_{ab}^R(\eta, \eta_{\text{in}}, k)$ is subject to the defining equation

$$\left[\partial_\eta \delta_{ab} + \Omega_{ab}(\eta, k) \right] g_{bc}^R(\eta, \eta_{\text{in}}, k) = \delta_{ac} \delta_{\text{D}}^{(1)}(\eta - \eta_{\text{in}}), \quad (3.6)$$

together with the causal boundary conditions

$$\begin{aligned} g_{ab}^R(\eta, \eta_{\text{in}}, k) &= 0 & \text{for } \eta < \eta_{\text{in}}, \\ g_{ab}^R(\eta, \eta_{\text{in}}, k) &\rightarrow \delta_{ab} & \text{for } \eta \rightarrow \eta_{\text{in}}^+, \end{aligned} \quad (3.7)$$

and henceforth called the retarded linear propagator. The function $R(\eta)$ can be rewritten to

$$\begin{aligned} R(\eta) = \frac{4\pi}{3} \int_0^\infty \frac{dq q^2}{(2\pi)^3} \left[-g_{3a_s}^R(\eta, \eta_{\text{in}}, q) + 2g_{4a_s}^R(\eta, \eta_{\text{in}}, q) \right] g_{2b_s}^R(\eta, \eta_{\text{in}}, q) \\ \times w_{a_s}(q) w_{b_s}(q) P_s^{\text{in}}(q), \end{aligned} \quad (3.8)$$

which depends at linear level on the scalar retarded linear propagator only, due to the assumption of vanishing initial vector fluctuations. It is particularly convenient to discuss solutions in terms of the linear growth functions

$$D_a(\eta, k) \equiv g_{ab}^R(\eta, \eta_{\text{in}}, k) w_b(k), \quad (3.9)$$

⁵By definition (2.48) the initial time evolution parameter is $\eta_{\text{in}} \equiv 0$.

and the linear transfer function

$$T_{ab}^2(\eta, k) \equiv D_a(\eta, k) D_b(\eta, k), \quad (3.10)$$

such that the equal-time linear evolved scalar power spectra can be written as

$$P_{a_s b_s}(\eta, k) = T_{a_s b_s}^2(\eta, k) P_s^{\text{in}}(k), \quad (3.11)$$

where the vector and tensor components of $w_a(k)$ may be arbitrarily chosen as long as the vector and tensor initial fields vanish.

We emphasise that equation (3.6) is non-linear and the retarded linear propagator is not a Green's function in the standard sense of linear differential equations. It depends on the initial velocity dispersion background and is a functional of the initial scalar power spectrum as well as $w_{a_s}(k)$. As a consequence, the linear fields do not grow independently for different Fourier modes in contrast to the single-stream approximation, because $R(\eta)$ is sensitive to the evolution of the fields for all wave numbers k . Nevertheless, equation (3.5) can be seen as a *linear* response to a *small* perturbation in the initial random field.

Since $\Omega_{ab}(\eta, k)$ is block diagonal for scalar, vector and tensor fields, and because $R(\eta)$ depends on $g_{a_s b_s}^R(\eta, \eta_{\text{in}}, k)$ only, we can solve the scalar part of equation (3.6) together with the velocity dispersion background (3.2) independent from the vector and tensor parts. Subsequently the vector and tensor part can be solved.

3.2 Scalar growth factors and free-streaming scale

Because $g_{a_s b_s}^R(\eta, \eta_{\text{in}}, k)$ depends $w_{a_s}(k)$, we need to specify the latter in order to solve the scalar part of equation (3.6). To make a sensible choice we consider the eigenvalues of the submatrix $-\Omega_{a_s b_s}(\eta, k)$ which determine the growth of the solutions and are henceforth called growth factors. Three growth factors are given by the roots of the polynomial

$$\left[s_s(\eta, k) - 1 \right] \left[s_s(\eta, k) + \frac{3}{2} \right] \left[s_s(\eta, k) + R(\eta) \right] + k^2 \hat{\sigma}(\eta) \left[3 s_s(\eta, k) + R(\eta) \right], \quad (3.12)$$

whereas the fourth is $s_s(\eta, k) = -R(\eta)$. In the limit of small wave number $k \rightarrow 0$, one can easily find the roots of the polynomial (3.12) and obtains

$$\begin{aligned} s_s^{(1)}(\eta, k) &= 1 + \mathcal{O}(k^2), & s_s^{(2)}(\eta, k) &= -\frac{3}{2} + \mathcal{O}(k^2), \\ s_s^{(3)}(\eta, k) &= -R(\eta) + \mathcal{O}(k^2), & s_s^{(4)}(\eta, k) &= -R(\eta). \end{aligned} \quad (3.13)$$

To fully characterise the solutions the corresponding eigenvectors are needed. These are given by

$$v_{a_s}^{(n)}(\eta, k) = \begin{pmatrix} 1 \\ s_s^{(n)}(\eta, k) \\ \frac{2 s_s^{(n)}(\eta, k)}{3 (s_s^{(n)}(\eta, k) + R(\eta))} \\ \frac{4 s_s^{(n)}(\eta, k)}{3 (s_s^{(n)}(\eta, k) + R(\eta))} \end{pmatrix}, \quad v_{a_s}^{(4)}(\eta, k) = \begin{pmatrix} 0 \\ 0 \\ -1 \\ 1 \end{pmatrix}, \quad (3.14)$$

for $n \in \{1, 2, 3\}$. The eigenvectors (3.14) depend on $R(\eta)$ due to the non-linearity of equation (3.6).

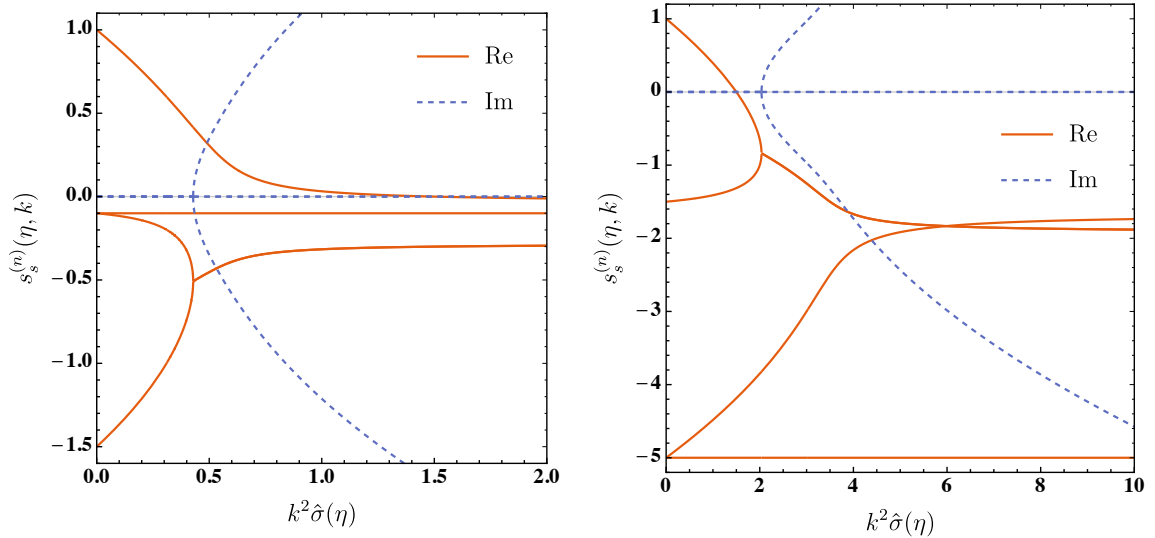


Figure 1. Growth factors $s_s^{(n)}(\eta, k)$ of the scalar fluctuation fields for $n \in \{1, 2, 3, 4\}$ as a function of the combination $k^2 \hat{\sigma}(\eta)$ for positive values of $R(\eta)$. The left panel shows the growth factors for $R(\eta) = 1/10$ while the right panel is for $R(\eta) = 5$. See text for further discussion.

In the formal limit $k \rightarrow 0$, the density and velocity-divergence fields obey the dynamics of the single-stream approximation. In turn the density and velocity-divergence components of $g_{a_s b_s}^R(\eta, \eta_{\text{in}}, k)$ obey a growing and decaying solution proportional to $e^{\eta - \eta_{\text{in}}}$ and $e^{-\frac{3}{2}(\eta - \eta_{\text{in}})}$, respectively [74]. In this limit $s_s^{(1)}(\eta, 0)$ and $s_s^{(2)}(\eta, 0)$ can be identified with these solutions, whereas $s_s^{(3)}(\eta, 0)$ and $s_s^{(4)}(\eta, 0)$ correspond to two new solutions which can be excited due to the presence of the scalar velocity dispersion fields.

For finite values of $k^2 \hat{\sigma}(\eta)$ the picture is more complicated and also depends on $R(\eta)$. In figure 1 we show the real and imaginary parts of $s_s^{(n)}(\eta, k)$ for $n \in \{1, 2, 3, 4\}$ as a function of the combination $k^2 \hat{\sigma}(\eta)$ for two different values of $R(\eta)$. These cover the qualitative behaviour for all $R(\eta) > 0$, which is the case we are finally interested in. For completeness, the case $R(\eta) < 0$ is discussed in appendix A.

For $R(\eta) > 0$ the only positive growth factor is $s_s^{(1)}(\eta, k)$ in the range $0 \leq k^2 \hat{\sigma}(\eta) < 3/2$. For $0 < R(\eta) < 9/2$ the growth factor $s_s^{(1)}(\eta, k)$ is real for all $k^2 \hat{\sigma}(\eta)$ and turns negative for $3/2 < k^2 \hat{\sigma}(\eta) < \infty$. The growth factors $s_s^{(2)}(\eta, k)$ and $s_s^{(3)}(\eta, k)$ develop an imaginary part at some $k^2 \hat{\sigma}(\eta) > 0$ from where on their real parts stay negative and coincide. This is shown in the left panel of figure 1 for $R(\eta) = 1/10$. For $9/2 \leq R(\eta) < \infty$ we find that $s_s^{(1)}(\eta, k)$ turns negative at $k^2 \hat{\sigma}(\eta) = 3/2$ and subsequently develops an imaginary part for larger $k^2 \hat{\sigma}(\eta)$. From there on the real part coincides with the real part of $s_s^{(2)}(\eta, k)$ which also develops an imaginary part while $s_s^{(3)}(\eta, k)$ is real and negative for all $k^2 \hat{\sigma}(\eta)$. This is shown in the right panel of figure 1 for $R(\eta) = 5$.

Since we are interested in growing solutions of equation (3.6) we concentrate in the following on the natural extension of the solution characterised by the growth factor $s_s^{(1)}(\eta, k)$ when terms at finite k are restored. We assume that initially only the growing solution is present and the corresponding eigenvector determines the initial scalar fields, i.e.

$$w_{a_s}(k) = v_{a_s}^{(1)}(\eta_{\text{in}}, k). \quad (3.15)$$

Due to the dependence of $v_{a_s}^{(1)}(\eta_{\text{in}}, k)$ on the value $R(\eta_{\text{in}})$ one needs to compute

$$R(\eta_{\text{in}}) = \frac{4\pi}{3} \int_0^\infty \frac{dq q^2}{(2\pi)^3} \left[-w_3(q) + 2w_4(q) \right] w_2(q) P_s^{\text{in}}(q), \quad (3.16)$$

simultaneously. For the growing solution, an initial scalar power spectrum as specified in section 4.1 implies $R(\eta_{\text{in}}) > 0$.

Before solving the system of equations (3.2) and (3.6) by numerical means, it is sensible to infer some properties of the growing solution. The real part of the growth factor $s_s^{(1)}(\eta, k)$ is a monotonically decreasing function of k and has a zero-crossing at the comoving free-streaming wave number

$$k_{\text{fs}}(\eta) \equiv \sqrt{\frac{3}{2\hat{\sigma}(\eta)}}. \quad (3.17)$$

As discussed above, $s_s^{(1)}(\eta, k)$ is negative for all $k > k_{\text{fs}}(\eta)$ and, for $R(\eta) \geq 9/2$, subsequently develops an imaginary part. The corresponding solution is damped at large wave numbers and starts oscillating. Therefore $k_{\text{fs}}(\eta)$ determines the scale below which the fluctuation fields do not grow due to the free-streaming of dark matter particles. In order to qualitatively understand how $k_{\text{fs}}(\eta)$ evolves in time, we consider the limit of early and late times. At early times the fluctuation fields are small in amplitude and one can neglect the enhancement of the velocity dispersion background (3.2) due to $R(\eta)$ as long as

$$\int_{\eta_{\text{in}}}^{\eta} d\xi R(\xi) \ll \eta - \eta_{\text{in}}. \quad (3.18)$$

In this limit $\hat{\sigma}(\eta)$ decays in time and in turn the free-streaming wave number is raised which allows structures to form at smaller scales. At later times, however, the fluctuation fields grow in amplitude and the validity of the limit (3.18) breaks down. Eventually, at times where

$$\int_{\eta_{\text{in}}}^{\eta} d\xi R(\xi) > \eta - \eta_{\text{in}}, \quad (3.19)$$

the velocity dispersion background starts to grow and in turn $k_{\text{fs}}(\eta)$ decays which stalls the formation of structure at small scales.

3.3 Vector and tensor growth factors

Similar to the case of scalar fields it is sensible to study properties of the vector field propagator $g_{a_v b_v}^R(\eta, \eta_{\text{in}}, k)$ in terms of the eigenvalues of the submatrix $-\Omega_{a_v b_v}(\eta, k)$. The growth factors for the vector fields are given by

$$\begin{aligned} s_v^{(1)}(\eta, k) &= -\frac{1 + 2R(\eta)}{4} - \sqrt{\left(\frac{1 - 2R(\eta)}{4}\right)^2 - k^2 \hat{\sigma}(\eta)}, \\ s_v^{(2)}(\eta, k) &= -\frac{1 + 2R(\eta)}{4} + \sqrt{\left(\frac{1 - 2R(\eta)}{4}\right)^2 - k^2 \hat{\sigma}(\eta)}, \end{aligned} \quad (3.20)$$

and the corresponding eigenvectors are

$$v_{a_v}^{(n)}(\eta, k) = \begin{pmatrix} -s_v^{(n)}(\eta, k) - R(\eta) \\ 1 \end{pmatrix}, \quad (3.21)$$

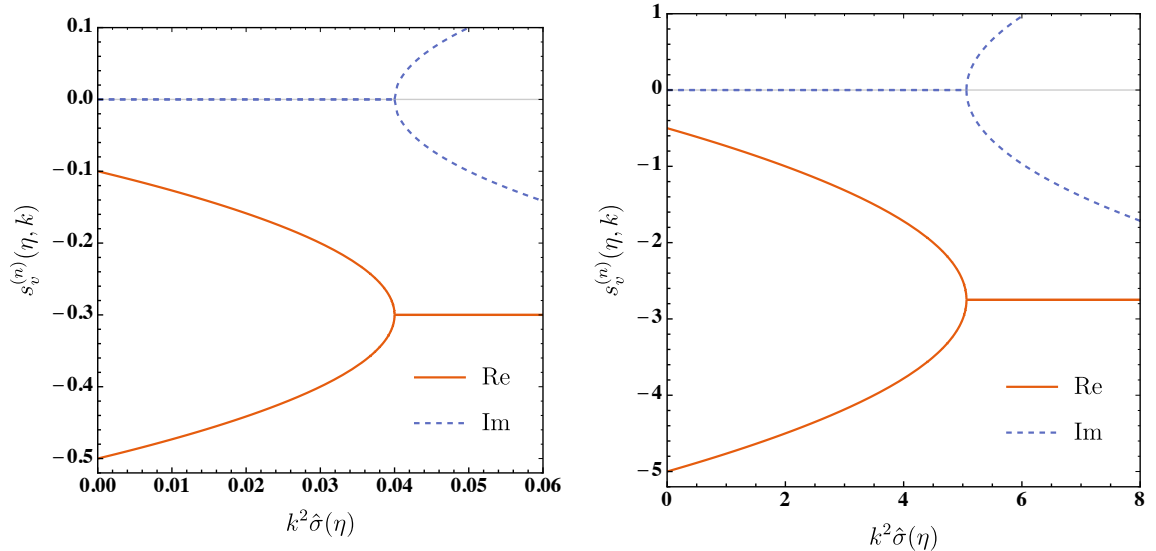


Figure 2. Growth factors $s_v^{(n)}(\eta, k)$ of the vector fluctuation fields for $n \in \{1, 2\}$ as a function of the combination $k^2 \hat{\sigma}(\eta)$ for positive values of $R(\eta)$. The left panel shows the growth factors for $R(\eta) = 1/10$ while the right panel is for $R(\eta) = 5$. See text for further discussion.

for $n \in \{1, 2\}$. In the limit of small wave numbers $k \rightarrow 0$ these are

$$s_v^{(1)}(\eta, k) = -\frac{1}{2} + \mathcal{O}(k^2), \quad s_v^{(2)}(\eta, k) = -R(\eta) + \mathcal{O}(k^2). \quad (3.22)$$

Since the formal limit $k \rightarrow 0$ restores the equations of motion of the single-stream approximation by decoupling the vorticity field from the vector velocity dispersion field, we can identify $s_v^{(1)}(\eta, 0)$ with the decaying solution of the vorticity field proportional to $e^{-\frac{1}{2}(\eta - \eta_{\text{in}})}$. The growth factor $s_v^{(2)}(\eta, k)$ corresponds to a new solution which can be excited due to the presence of the vector velocity dispersion fields.

For finite values of $k^2 \hat{\sigma}(\eta)$, the real and imaginary parts of $s_v^{(n)}(\eta, k)$ for $n \in \{1, 2\}$ are shown in figure 2 for two different values of $R(\eta)$ which cover the qualitative behaviour of the growth factors for all $R(\eta) > 0$. The case $R(\eta) < 0$ is discussed in appendix A. For $0 < R(\eta) < \infty$ both growth factors $s_v^{(1)}(\eta, k)$ and $s_v^{(2)}(\eta, k)$ are real and negative for sufficient small $k^2 \hat{\sigma}(\eta)$. For larger $k^2 \hat{\sigma}(\eta)$ they develop an imaginary part from where on their real parts coincide and take a constant negative value. In the range $0 < R(\eta) < 1/2$ the growth factor $s_v^{(1)}(\eta, k)$ is monotonically increasing while $s_v^{(2)}(\eta, k)$ is monotonically decreasing for larger $k^2 \hat{\sigma}(\eta)$ until it develops an imaginary part. This is shown in the left panel of figure 2 for $R(\eta) = 1/10$. For $1/2 < R(\eta) < \infty$ the growth is reversed such that $s_v^{(1)}(\eta, k)$ is monotonically decreasing and $s_v^{(2)}(\eta, k)$ is monotonically increasing for larger $k^2 \hat{\sigma}(\eta)$ as long as these are real. This is shown in the right panel of figure 2 for $R(\eta) = 5$.

Because the vector part of equation (3.6) is a first-order linear ordinary differential equation, any general solution can be constructed by superposition of the solutions characterised by the growth factors $s_v^{(n)}(\eta, k)$ for $n \in \{1, 2\}$.⁶ The corresponding initial conditions are

⁶This is only true as long as we neglect initial vector fields which would enter $R(\eta)$ by definition (2.56) and thus couple the scalar and vector part of equation (3.6).

determined by the initial eigenvectors, i.e.

$$w_{a_v}^{(n)}(k) = v_{a_v}^{(n)}(\eta_{\text{in}}, k). \quad (3.23)$$

Finally, the tensor part of equation (3.6) together with the submatrix (2.60) is independent of k and the tensor retarded linear propagator is therefore given by

$$g_{a_t b_t}^R(\eta, \eta_{\text{in}}, k) = \exp \left\{ - \int_{\eta'}^{\eta} d\xi R(\xi) \right\}. \quad (3.24)$$

The corresponding tensor growth factor is $s_t(\eta, k) = -R(\eta)$ for which we simply chose $w_{a_t}(k) = 1$ as the initial tensor field configuration.

3.4 Approximation for small velocity dispersion and soft power spectrum

In the following we discuss an approximate analytical solution that becomes available in the limit where the velocity dispersion background $\hat{\sigma}(\eta)$ is small and where the initial scalar power spectrum $P_s^{\text{in}}(k)$ does not extend too far into the ultraviolet, in a sense that becomes clear below.

Assuming that the velocity dispersion background $\hat{\sigma}(\eta)$ is small, we consider the evolution of the decomposed fluctuation fields at wave numbers $k^2 \hat{\sigma}(\eta) \ll 1$. Since their evolution depends on $R(\eta)$, which involves an integral over all wave numbers, this assumption does on first sight not seem sensible. However, as discussed in section 4, the initial scalar power spectrum $P_s^{\text{in}}(k)$ is heavily suppressed for wave numbers larger than the comoving free-streaming wave number at matter-radiation equality $k_{\text{fs,eq}}$. The above proposed approximation can therefore be used as long as $k_{\text{fs,eq}}^2 \hat{\sigma}(\eta) \ll 1$.

By dropping the $k^2 \hat{\sigma}(\eta)$ terms in the matrix $\Omega_{ab}(\eta, k)$ and denoting objects in the approximation by a tilde, equation (3.6) can be written in terms of linear growth functions,

$$\left[\partial_\eta \delta_{ab} + \tilde{\Omega}_{ab}(\eta) \right] \tilde{D}_b(\eta) = w_a(0) \delta_{\text{D}}^{(1)}(\eta - \eta_{\text{in}}), \quad (3.25)$$

where $\tilde{\Omega}_{ab}(\eta)$ is block diagonal for scalar, vector and tensor fields and given by the submatrices

$$\tilde{\Omega}_{a_s b_s}(\eta) \equiv \begin{pmatrix} 0 & -1 & 0 & 0 \\ -\frac{3}{2} & \frac{1}{2} & 0 & 0 \\ 0 & -\frac{2}{3} & \tilde{R}(\eta) & 0 \\ 0 & -\frac{4}{3} & 0 & \tilde{R}(\eta) \end{pmatrix}, \quad \tilde{\Omega}_{a_v b_v}(\eta) \equiv \begin{pmatrix} \frac{1}{2} & 0 \\ 1 & \tilde{R}(\eta) \end{pmatrix}, \quad \tilde{\Omega}_{a_t b_t}(\eta) \equiv \tilde{R}(\eta). \quad (3.26)$$

The function (3.8) takes the form

$$\tilde{R}(\eta) = \frac{\sigma_d^2}{3} \left[-\tilde{D}_3(\eta) + 2\tilde{D}_4(\eta) \right] \tilde{D}_2(\eta), \quad (3.27)$$

where

$$\sigma_d^2 \equiv 4\pi \int_0^\infty \frac{dq q^2}{(2\pi)^3} P_s^{\text{in}}(q), \quad (3.28)$$

is the dimensionless variance of the initial density fluctuation field and is the only quantity appearing in the approximation which is sensitive to the initial scalar power spectrum.⁷

⁷Notice the difference to the single-stream approximation which depends even at one-loop level only on the dimensionful parameter $\sigma_v^2 \equiv 4\pi/3 \int_0^\infty dq P_s^{\text{in}}(q)/(2\pi)^3$ [75]. For a perfectly cold dark matter power spectrum as in equation (4.1), the integral (3.28) diverges approximately logarithmically.

The initial conditions are given by the $k \rightarrow 0$ limit of the initial field configuration $w_a(k)$ specified in section 3.2 and 3.3. For scalar fields corresponding to the growing solution with $s_s^{(1)}(\eta, 0) = 1$ these are given by

$$w_{a_s}(0) = \begin{pmatrix} 1 \\ 1 \\ 2 \\ \frac{3(1 + \tilde{R}(\eta_{\text{in}}))}{4} \\ \frac{3(1 + \tilde{R}(\eta_{\text{in}}))}{4} \end{pmatrix}. \quad (3.29)$$

The vector fields corresponding to $s_v^{(1)}(\eta, 0) = -1/2$ and $s_v^{(2)}(\eta, 0) = -R(\eta)$ are excited by

$$w_{a_v}^{(1)}(0) = \begin{pmatrix} \frac{1}{2} - \tilde{R}(\eta_{\text{in}}) \\ 1 \end{pmatrix}, \quad w_{a_v}^{(2)}(0) = \begin{pmatrix} 0 \\ 1 \end{pmatrix}, \quad (3.30)$$

respectively and for the tensor field corresponding to $s_t(\eta, 0) = -R(\eta)$ we use $w_{a_t}(0) = 1$.

The initial value of $\tilde{R}(\eta)$ can be calculated using the initial scalar field configuration (3.29) and is given by

$$\tilde{R}(\eta_{\text{in}}) = -\frac{1}{2} \pm \sqrt{\frac{1}{4} + \frac{2\sigma_d^2}{3}}, \quad (3.31)$$

where, as discussed in section 3.2, the positive solution needs to be picked for consistency. Finally, to close the system of equations (3.25) the velocity dispersion background

$$\tilde{\sigma}(\eta) = \hat{\sigma}_{\text{in}} \exp \left\{ \int_{\eta_{\text{in}}}^{\eta} d\xi (\tilde{R}(\xi) - 1) \right\}, \quad (3.32)$$

is needed.

The linear growth functions of the density and velocity-divergence fields obey the growing solution

$$\tilde{D}_1(\eta) = e^{\eta - \eta_{\text{in}}}, \quad \tilde{D}_2(\eta) = e^{\eta - \eta_{\text{in}}}, \quad (3.33)$$

while the scalar velocity dispersion linear growth functions are

$$\tilde{D}_3(\eta) = \frac{2}{3C_1} \tanh(H_1(\eta)), \quad \tilde{D}_4(\eta) = \frac{4}{3C_1} \tanh(H_1(\eta)). \quad (3.34)$$

Here we defined the function

$$H_1(\eta) \equiv C_1 (e^{\eta - \eta_{\text{in}}} - 1) + \text{artanh}(C_2), \quad (3.35)$$

where

$$C_1 \equiv \sqrt{\frac{2\sigma_d^2}{3}}, \quad C_2 \equiv \frac{\sqrt{24\sigma_d^2}}{3 + \sqrt{9 + 24\sigma_d^2}}, \quad (3.36)$$

are real positive constants with $C_2 < 1$. The vorticity field linear growth function is given by

$$\tilde{D}_5^{(n)}(\eta) = w_5^{(n)}(0) e^{-\frac{1}{2}(\eta - \eta_{\text{in}})}, \quad (3.37)$$

and the vector velocity dispersion linear growth function is

$$\tilde{D}_6^{(n)}(\eta) = \frac{\text{sech}(H_1(\eta))}{\sqrt{1-C_2^2}} \left[w_6^{(n)}(0) + 2 w_5^{(n)}(0) \left(H_2(\eta) e^{-\frac{1}{2}(\eta-\eta_{\text{in}})} + H_3(\eta) - 1 \right) \right], \quad (3.38)$$

for $n \in \{1, 2\}$. Here we introduced the functions

$$H_2(\eta) \equiv \cosh(C_1 (e^{\eta-\eta_{\text{in}}} - 1)) + C_2 \sinh(C_1 (e^{\eta-\eta_{\text{in}}} - 1)), \quad (3.39)$$

and

$$H_3(\eta) \equiv \sqrt{C_1} (1 - C_2) e^{C_1} \left[\frac{\sqrt{\pi}}{2} \text{erf}\left(\sqrt{C_1} e^{\frac{1}{2}(\eta-\eta_{\text{in}})}\right) - \frac{\sqrt{\pi}}{2} \text{erf}\left(\sqrt{C_1}\right) \right] \\ - \sqrt{C_1} (1 + C_2) e^{-C_1} \left[\frac{\sqrt{\pi}}{2} \text{erfi}\left(\sqrt{C_1} e^{\frac{1}{2}(\eta-\eta_{\text{in}})}\right) - \frac{\sqrt{\pi}}{2} \text{erfi}\left(\sqrt{C_1}\right) \right], \quad (3.40)$$

where $\text{erf}(x)$ and $\text{erfi}(x)$ denote the real and imaginary error function, respectively. The tensor velocity dispersion linear growth function has the solution

$$\tilde{D}_7(\eta) = \frac{\text{sech}(H_1(\eta))}{\sqrt{1-C_2^2}}, \quad (3.41)$$

which coincides with $\tilde{D}_6^{(2)}(\eta)$. Finally, the velocity dispersion background is given by

$$\tilde{\sigma}(\eta) = \hat{\sigma}_{\text{in}} e^{-(\eta-\eta_{\text{in}})} H_2(\eta). \quad (3.42)$$

With the analytical solutions (3.33), (3.34), (3.37), (3.38), (3.41) and (3.42) we can infer the early and late time behaviour of the linear growth functions and velocity dispersion background in the approximative scenario.

As for the single-stream approximation, the density and velocity-divergence fields grow at all times exponentially with the time evolution parameter $\eta - \eta_{\text{in}}$. In contrast, the scalar velocity dispersion fields grow at early times $\eta - \eta_{\text{in}} \ll 1$ exponentially,

$$\tilde{D}_3(\eta) \propto e^{\eta-\eta_{\text{in}}}, \quad \tilde{D}_4(\eta) \propto e^{\eta-\eta_{\text{in}}}, \quad (3.43)$$

while at late times they asymptotically approach a finite value. In the formal limit $\eta - \eta_{\text{in}} \rightarrow \infty$ we find

$$\tilde{D}_3(\eta) \rightarrow \sqrt{\frac{2}{3\sigma_d^2}}, \quad \tilde{D}_4(\eta) \rightarrow \sqrt{\frac{8}{3\sigma_d^2}}. \quad (3.44)$$

Note that the values (3.44) are consistent with the cold dark matter limit $\sigma_d^2 \rightarrow \infty$ which implies vanishing velocity dispersion fields. The vector and tensor linear growth functions decay at all times and vanish in the late time limit.

According to the definitions (2.17), (2.27), (2.28), (2.29), (2.30) and (2.52) the velocity dispersion linear growth functions describe perturbations relative to the velocity dispersion background. The latter is therefore needed for a complete picture. According to the approximation (3.42) it decays exponentially at early times,

$$\tilde{\sigma}(\eta) \propto e^{-(\eta-\eta_{\text{in}})}, \quad (3.45)$$

while at late times one finds in the formal limit $\eta - \eta_{\text{in}} \rightarrow \infty$ the dominant behaviour to be a double exponential growth,

$$\tilde{\sigma}(\eta) \propto \exp\left\{C_1 e^{\eta-\eta_{\text{in}}} - (\eta - \eta_{\text{in}})\right\}. \quad (3.46)$$

This qualitatively agrees with the early and late times regimes (3.18) and (3.19) discussed in section 3.2.

4 Numerical results

h	$\Omega_{c,0} h^2$	$\Omega_{b,0} h^2$	z_{re}	A_s	n_s
0.6774	0.1188	0.0223	8.8	$2.142 \cdot 10^{-9}$	0.9667

Table 1. Cosmological parameters found by the Planck Collaboration [77] where h is the reduced Hubble constant, $\Omega_{c,0}$ and $\Omega_{b,0}$ are the current cold dark matter and baryonic matter density parameters respectively, z_{re} is the redshift at reionisation, A_s is the primordial scalar amplitude at the pivot scale $k_* = 0.05 h/\text{Mpc}$ and n_s is the scalar spectral index.

4.1 Initial scalar power spectrum and velocity dispersion background

To solve the system of equations (3.2) and (3.6) numerically we need to specify the velocity dispersion background $\hat{\sigma}_{\text{in}}$ as well as the scalar power spectrum $P_s^{\text{in}}(k)$ at an initial time τ_{in} . We set τ_{in} deep within the matter dominated era of the Universe at a redshift of $z(\tau_{\text{in}}) \equiv 1/a(\tau_{\text{in}}) - 1 = 100$ and assume that the non-linear evolution of perturbations is negligible at earlier times, such that we can use a linearly evolved power spectrum as initial condition. Further we assume that the matter fluctuation fields are initially small enough in amplitude to be in the regime (3.18) where the velocity dispersion background simply decays in time.

We generate a linear evolved cold dark matter scalar power spectrum $P_{\text{CDM}}(k)$ using the CLASS code [76] for wave numbers $k \in [10^{-5}, 10] h/\text{Mpc}$ assuming a ΛCDM cosmology using the parameters given in table 1. To extrapolate to smaller and larger wave numbers we use the prominent Eisenstein & Wu fitting formula [78]

$$P_{\text{CDM}}(k) = \alpha k^{n_s} \frac{L^2(k)}{(L(k) + C(k) (\beta k)^2)^2}, \quad (4.1)$$

where

$$L(k) = \ln(e + 1.84 \beta k), \quad C(k) = 14.4 + \frac{325}{1 + 60.5 (\beta k)^{1.11}}, \quad (4.2)$$

and α, β, e are real positive constants.

For dark matter of non-vanishing velocity dispersion, structure formation is stalled at small scales due to free-streaming of dark matter particles. In the matter dominated era, structures are erased for wave numbers larger than the comoving free-streaming wave number at matter-radiation equality $k_{\text{fs,eq}}$ [79]. For $k \lesssim k_{\text{fs,eq}}$ the warm dark matter transfer function is in leading approximation given by

$$T_{\text{WDM}}(k) = 1 - \left(\frac{\gamma(k)}{\gamma_0} \right)^2, \quad (4.3)$$

where $\gamma(k) \equiv \sqrt{2} k/k_{\text{fs,eq}}$ and $\gamma_0 \equiv \sqrt{63/31}$ [80]. For wave numbers $k \gtrsim k_{\text{fs,eq}}$ the transfer function strongly suppresses the power spectrum and for simplicity we employ an ultraviolet cutoff $\Lambda \equiv \gamma_0/\sqrt{2} k_{\text{fs,eq}}$ at the zero-crossing of the transfer function (4.3). The initial scalar power spectrum is then given by

$$P_s^{\text{in}}(k) = T_{\text{WDM}}^2(k) \Theta_{\text{H}}^{(1)}(\Lambda - k) P_{\text{CDM}}(k), \quad (4.4)$$

where $\Theta_{\text{H}}^{(n)}(x)$ denotes the n -dimensional Heaviside unit step function.

For our numerical investigations we consider two dark matter candidates, namely sterile neutrinos of mass $m \sim 1$ keV and weakly interacting massive particles (WIMPs) of mass $m \sim 100$ GeV. The free-streaming wave number and velocity dispersion background at matter-radiation equality are given by

$$k_{\text{fs,eq}} \approx 11 \frac{h}{\text{Mpc}}, \quad \hat{\sigma}_{\text{eq}} \approx 1.1 \cdot 10^{-2} \frac{\text{Mpc}^2}{h^2}, \quad (4.5)$$

for sterile neutrino dark matter and

$$k_{\text{fs,eq}} \approx 1.6 \cdot 10^7 \frac{h}{\text{Mpc}}, \quad \hat{\sigma}_{\text{eq}} \approx 5.5 \cdot 10^{-15} \frac{\text{Mpc}^2}{h^2}, \quad (4.6)$$

for WIMP dark matter [81]. We evolve the velocity dispersion background to τ_{in} using the evolution equation (2.57) in an Einstein-de Sitter cosmology ($\Omega_m(\tau) = 1$, $f(\tau) = 1$) and neglect the enhancement from $R(\eta)$. This approximation is sensible as long as the initial time τ_{in} is well within the matter dominated era and $R(\eta_{\text{in}}) \ll 1$. Indeed, for $z(\tau_{\text{in}}) = 100$ we find $R(\eta_{\text{in}}) \approx 0.002$ for sterile neutrino dark matter and $R(\eta_{\text{in}}) \approx 0.08$ for WIMP dark matter. The initial velocity dispersion background is then

$$\hat{\sigma}_{\text{in}} = \frac{a_{\text{eq}}}{a_{\text{in}}} \hat{\sigma}_{\text{eq}}, \quad (4.7)$$

where $a_{\text{eq}} \approx 1/3229$ is the scale factor at matter-radiation equality.

Having specified the initial conditions, the system of equations (3.2) and (3.6) can be solved with numerical methods. This becomes particularly involved when $k^2 \hat{\sigma}(\eta)$ is large and the approximation discussed in section 3.4 breaks down. Since we know from the discussion of the growth factor $s_s^{(1)}(\eta, k)$ that the scalar fluctuation fields are suppressed for $k \gg k_{\text{fs}}(\eta)$, we expect the ultraviolet modes to contribute less to the integral (3.8). Therefore we employ a maximal wavenumber

$$k_{\text{max}}(\eta) \equiv \sqrt{\frac{N}{\hat{\sigma}(\eta)}}, \quad (4.8)$$

where N is chosen such that $k_{\text{fs}}(\eta) \ll k_{\text{max}}(\eta) \leq \Lambda$. It determines up to which wave number we compute the fluctuation fields and in turn controls the accuracy of $R(\eta)$. In principle, we should take $k_{\text{max}}(\eta) \rightarrow \Lambda$ but this leads to strongly oscillating and difficult to control numerical integrals at late times. In this sense $k_{\text{max}}(\eta) < \Lambda$ implies an approximation and therefore the numerical solutions need to be taken with a grain of salt.

Before proceeding to the numerical results we comment on the similarities and differences to the approach of reference [67]. There, a non-vanishing velocity dispersion expectation value was taken into account and the velocity dispersion degrees of freedom were parametrised with one scalar field only, corresponding to $(\zeta(\tau, \mathbf{k}) + \vartheta(\tau, \mathbf{k}))/2$ for $\mathbf{k} \neq 0$. The equations of motion for the resulting three scalar fields, namely density, velocity-divergence and scalar velocity dispersion, are approximated by neglecting the terms which involve the velocity dispersion background, similar to the approximation we introduced in section 3.4. In contrast to our current description with no interaction between Fourier modes, reference [67] took the standard vertices $A_{\theta\delta}(\mathbf{k}_1, \mathbf{k}_2)$, $B_{\theta\theta}(\mathbf{k}_1, \mathbf{k}_2)$ as well as the new vertices $D_{\zeta\theta}(\mathbf{k}_1, \mathbf{k}_2)$, $D_{\vartheta\theta}(\mathbf{k}_1, \mathbf{k}_2)$, $E_{\zeta\theta}(\mathbf{k}_1, \mathbf{k}_2)$ and $E_{\vartheta\theta}(\mathbf{k}_1, \mathbf{k}_2)$ corresponding to their parametrisation of the scalar velocity dispersion field into account. Summarising, their computation was done including

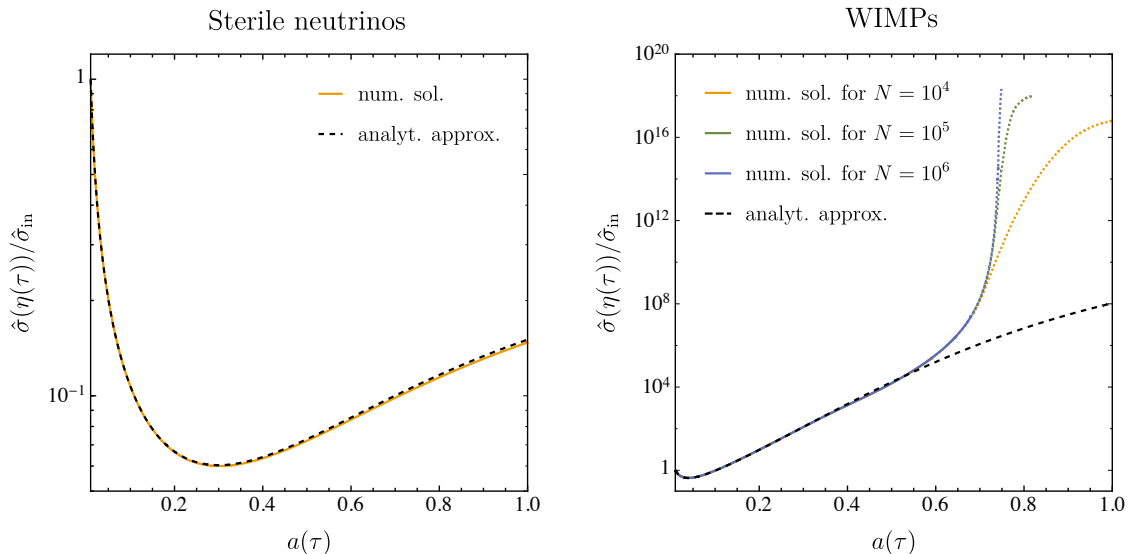


Figure 3. The velocity dispersion background $\hat{\sigma}(\eta)$ defined through equations (2.11), (2.16) and (2.55) normalised to unity at initial redshift $z(\tau_{\text{in}}) = 100$ as a function of the scale factor $a(\tau)$ for sterile neutrino (left panel) and WIMP (right panel) dark matter. The solid yellow, green and blue lines show the numerical solution (3.2) for different maximal reconstruction wave numbers (4.8) and the dotted lines indicate the regime where the artificial cutoff applies. The dashed black lines show the analytical approximation (3.42).

the enhancement of the velocity dispersion background due to parts of the scalar velocity dispersion degrees of freedom and the interaction of scalar Fourier modes, while back-reaction effects from the velocity dispersion background to the fluctuation fields were not accounted for. As they find, the velocity dispersion background undergoes an immense growth hinting to the fact that at late times this back-reaction can no longer be neglected. We take these back-reaction effects into account, in the sense that we keep the $k^2\hat{\sigma}(\eta)$ terms within the equations of motion which are linear in the fluctuation fields.

4.2 Results

In figure 3 we show the velocity dispersion background $\hat{\sigma}(\eta)$ defined through equations (2.11), (2.16) and (2.55) as a function of the scale factor $a(\tau)$ normalised to the initial value $\hat{\sigma}_{\text{in}}$. For sterile neutrino dark matter we take $k_{\text{max}}(\eta) = \Lambda$ since the free-streaming wave number at matter-radiation equality (4.5) is fairly small and a computation including all wave numbers does not pose a challenge. Because $k^2\hat{\sigma}(\eta) \ll 1$ for all times and wave numbers we are interested in, the analytical approximation (3.42) (dashed black lines) describes the numerical solution (3.2) (solid yellow line) very well as shown in the left panel of figure 3. The initial decay has a turnover to growth at $a(\tau) \approx 0.3$ where the inequality (3.18) get violated. At late times, the impact of finite $k^2\hat{\sigma}(\eta)$ can be seen where the numerical solution is smaller than the analytical approximation due to the suppression of ultraviolet modes. These contribute less to $R(\eta)$ which in turn reduces the growth of $\hat{\sigma}(\eta)$. The final value at $a(0) = 1$, corresponding to today, is given by $\bar{\sigma}(0) \approx 5.7 \cdot 10^{-12} c^2$. For WIMP dark matter on the other hand we employ the maximal reconstruction wave number (4.8) for $N = 10^4$ (yellow line), $N = 10^5$ (green line) and $N = 10^6$ (blue line). This implies an artificial ultraviolet cutoff for the calculation of $R(\eta)$ in the late times regime. The resulting $\hat{\sigma}(\eta)$ is decaying for $a(\tau) \lesssim 0.04$ and

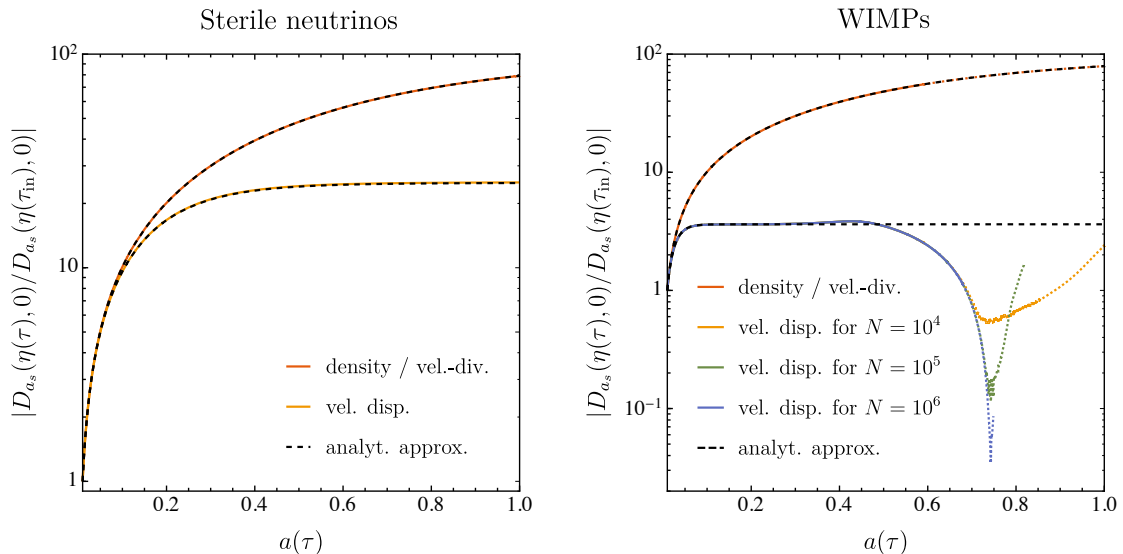


Figure 4. The scalar linear growth functions $D_{a_s}(\eta, k)$ defined in equation (3.9) in the small wave number limit $k \rightarrow 0$ normalised to unity at initial redshift $z(\tau_{\text{in}}) = 100$ as a function of the scale factor $a(\tau)$ for sterile neutrino (left panel) and WIMP (right panel) dark matter. The solid red, yellow, green and blue lines show the numerical solution of the scalar part of equation (3.6) corresponding to the growth factor $s_s^{(1)}(\eta, 0) = 1$ for different maximal reconstruction wave numbers (4.8). The dotted lines indicate the regime where the artificial cutoff (4.8) applies and the dashed black lines show the corresponding analytical approximations (3.33) and (3.34), respectively.

growing for all later times as shown in the right panel of figure 3. The turnover from decay to growth is earlier for WIMP dark matter than for sterile neutrino dark matter, because more ultraviolet modes are taken into account in the computation of $R(\eta)$ which in turn leaves the regime (3.18) much earlier. Similar to sterile neutrino dark matter, and for the same reasons, the numerical solution is smaller than the analytical approximation for intermediate times $0.29 \lesssim a(\tau) \lesssim 0.52$. However, for $a(\tau) \gtrsim 0.52$, $\hat{\sigma}(\eta)$ enters a phase of immense growth where it departs from the double exponential growth of the analytical approximation (3.46) by many orders of magnitude. Here the numerical computation of $R(\eta)$ is more challenging and we employ $k_{\text{max}}(\eta)$ smaller than the ultraviolet cutoff Λ of the initial state. The regime where this applies is indicated by dotted lines in the right panel of figure 3. More specifically, the artificial ultraviolet cutoff $k_{\text{max}}(\eta)$ applies with $N = 10^4$ for $a(\tau) \gtrsim 0.59$, with $N = 10^5$ for $a(\tau) \gtrsim 0.64$ and with $N = 10^6$ for $a(\tau) \gtrsim 0.68$. Since we are unable to evolve $\hat{\sigma}(\eta)$ to $a(0) = 1$ for $k_{\text{max}}(\eta) \rightarrow \Lambda$ we can only give the lower bound $\bar{\sigma}(0) \geq 3.9 \cdot 10^{-5} c^2$ on the final value, assuming the growth persists to later times. While the tremendous growth of $\hat{\sigma}(\eta)$ seems odd at first sight, it becomes clear from the discussion of the scalar linear transfer functions given in figures 6 and 7, which determine the growth of $R(\eta)$.

Before turning to the linear transfer functions, it is worthwhile to investigate the numerical solutions of equation (3.6) in the limit $k \rightarrow 0$. In the left panel of figure 4 the scalar linear growth functions $D_{a_s}(\eta, 0)$, defined by equation (3.9), corresponding to the growth function $s_s^{(1)}(\eta, 0) = 1$ are displayed for sterile neutrino dark matter. The density and velocity-divergence fields (red lines) grow exponentially because they obey the analytical approximation (3.33)

exactly in this limit. The scalar velocity dispersion fields (yellow lines) grow initially and approach a constant value at late times. As discussed above, the numerical solutions are well described by the analytical approximations (3.33) and (3.34) (dashed black lines). For WIMP dark matter the $D_{a_s}(\eta, 0)$ are shown in the right panel of figure 4. The behaviour is similar to the case of sterile neutrino dark matter at early times, but departs drastically in the regime where $\hat{\sigma}(\eta)$ undergoes extreme growth. In particular, the velocity dispersion fields (yellow, green and blue lines) depend on $R(\eta)$, which in turn is sensitive to the evolution of perturbations of all wave numbers and this results in an rapid decay at late times. Note that the dotted lines seem to indicate that velocity dispersion components of $D_{a_s}(\eta, 0)$ grow again at later times, but this is merely an artefact of the ultraviolet cutoff $k_{\text{max}}(\eta)$. Larger values of $k_{\text{max}}(\eta)$ lead to a longer lasting decay.

In figure 5, the vector linear growth functions $D_{a_v}^{(n)}(\eta, 0)$ corresponding to the growth factors $s_v^{(n)}(\eta, 0)$ for $n \in \{1, 2\}$, given in equation (3.20), are display for sterile neutrino (left panels) and WIMP (right panels) dark matter. In this limit, the k -independent tensor linear growth function $D_{a_t}(\eta, k)$ obeys the same dynamics as $D_{a_v}^{(2)}(\eta, 0)$ and we refrain from displaying the former separately. For the numerical solutions corresponding to $s_v^{(1)}(\eta, 0) = -1/2$ (upper panels of figure 5) the vorticity field (red line) is decaying exactly as the analytical approximation (3.37) (dashed black lines). In contrast, the vector velocity dispersion field (yellow, green and blue lines) initially decays in the same manner while at later times the decay is much stronger due to a growing $R(\eta)$ with a zero-crossing at $a(\tau) \approx 0.6$ for sterile neutrino dark matter and $a(\tau) \approx 0.1$ for WIMP dark matter. For the second independent solution (lower panels of figure 5), corresponding to $s_v^{(2)}(\eta, 0) = -R(\eta)$, only the vector velocity dispersion field is present for $k \rightarrow 0$ which is increasingly decaying due to $R(\eta)$. While the vector field behave qualitatively similar for sterile neutrino and WIMP dark matter, we observe a strong deviation from the analytical approximation at late times, similar to the scalar case.

In order to extract the relevant features, it is convenient to display the linear transfer functions $T_{ab}(\eta, k)$, defined through the equations (3.9) and (3.10), normalised to $T_{ab}(\eta, 0)$. In figures 6 and 7, we show $|T_{a_s b_s}(\eta, k)/T_{a_s b_s}(\eta, 0)|$ as a function of wave number k in units of the free-streaming wave number at matter-radiation equality $k_{\text{fs,eq}}$ at three different redshifts $z(\tau)$ for both dark matter species. The dependence of $T_{a_s b_s}(\eta, k)$ on k is qualitatively along the lines of the discussion of $s_s^{(1)}(\eta, k)$ in section 3.2. Because $s_s^{(1)}(\eta, k)$ is a monotonically decreasing function of $k^2 \hat{\sigma}(\eta)$, the scalar linear transfer functions are suppressed at late times and large k . For sterile neutrino dark matter the suppression is relatively modest because $\hat{\sigma}(\eta)$ is small and thus $k_{\text{fs}}(\eta)$ is large (left panels of figures 6 and 7). In the case of WIMP dark matter the scalar linear transfer functions show much more structure (right panels of figures 6 and 7). At late times, or small redshift, we find a strong suppression even for small k . For $k \gg k_{\text{fs}}(\eta)$ the scalar fields oscillate, triggered by a growth factor developing an imaginary part. In addition to the oscillation, we notice an amplification of the amplitude for the first few oscillations, at least for the velocity-divergence and scalar velocity dispersion fields. For larger k the amplitude decays as demanded by the negative real part of $s_s^{(1)}(\eta, k)$. Because the velocity-divergence and scalar velocity dispersion power spectra enter in the computation of $R(\eta)$, the enormous growth of $\hat{\sigma}(\eta)$ can be explained. For early times, the power spectra are only suppressed at large k and in turn $R(\eta)$ is smaller than the approximative counterpart $\tilde{R}(\eta)$. This is the regime where $\hat{\sigma}(\eta)$ is smaller than $\tilde{\sigma}(\eta)$. As soon as $R(\eta)$ is large enough

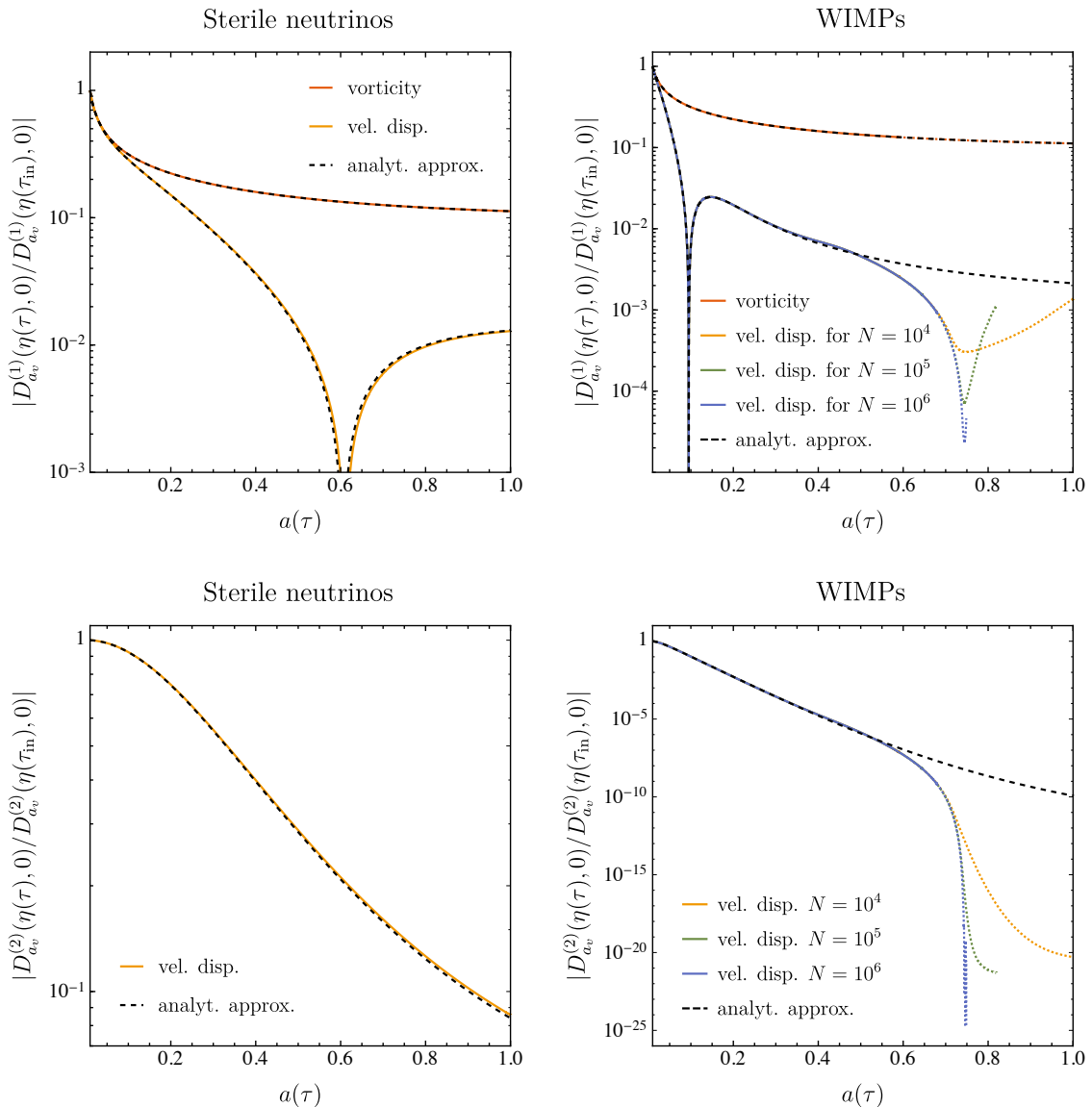


Figure 5. The vector linear growth functions $D_{a_v}^{(n)}(\eta, k)$ defined in equation (3.9) in the small wave number limit $k \rightarrow 0$ normalised to unity at initial redshift $z(\tau_{\text{in}}) = 100$ as a function of the scale factor $a(\tau)$ for sterile neutrino (left panels) and WIMP (right panels) dark matter. The solid red, yellow, green and blue lines show the numerical solution of the vector part of equation (3.6) corresponding to the growth factors $s_v^{(1)}(\eta, 0) = -1/2$ (upper panels) and $s_v^{(2)}(\eta, 0) = -R(\eta)$ (lower panels) for different maximal reconstruction wave numbers (4.8). The dotted lines indicate the regime where the artificial cutoff (4.8) applies and the dashed black lines show the corresponding analytical approximations (3.37) and (3.38), respectively.

for the fields to begin oscillating at large k the amplification of the first few oscillations compensate the suppression at larger k and even amplify $R(\eta)$. The amplification is larger for later times and thus results in a strong rise of $R(\eta)$. The latter in turn results in a strong growth of $\hat{\sigma}(\eta)$ and a decay of the scalar velocity dispersion fluctuation fields.

In figures 8 and 9 we show the transfer functions for the vector fields $|T_{a_v b_v}^{(n)}(\eta, k)/T_{a_v b_v}^{(n)}(\eta, 0)|$

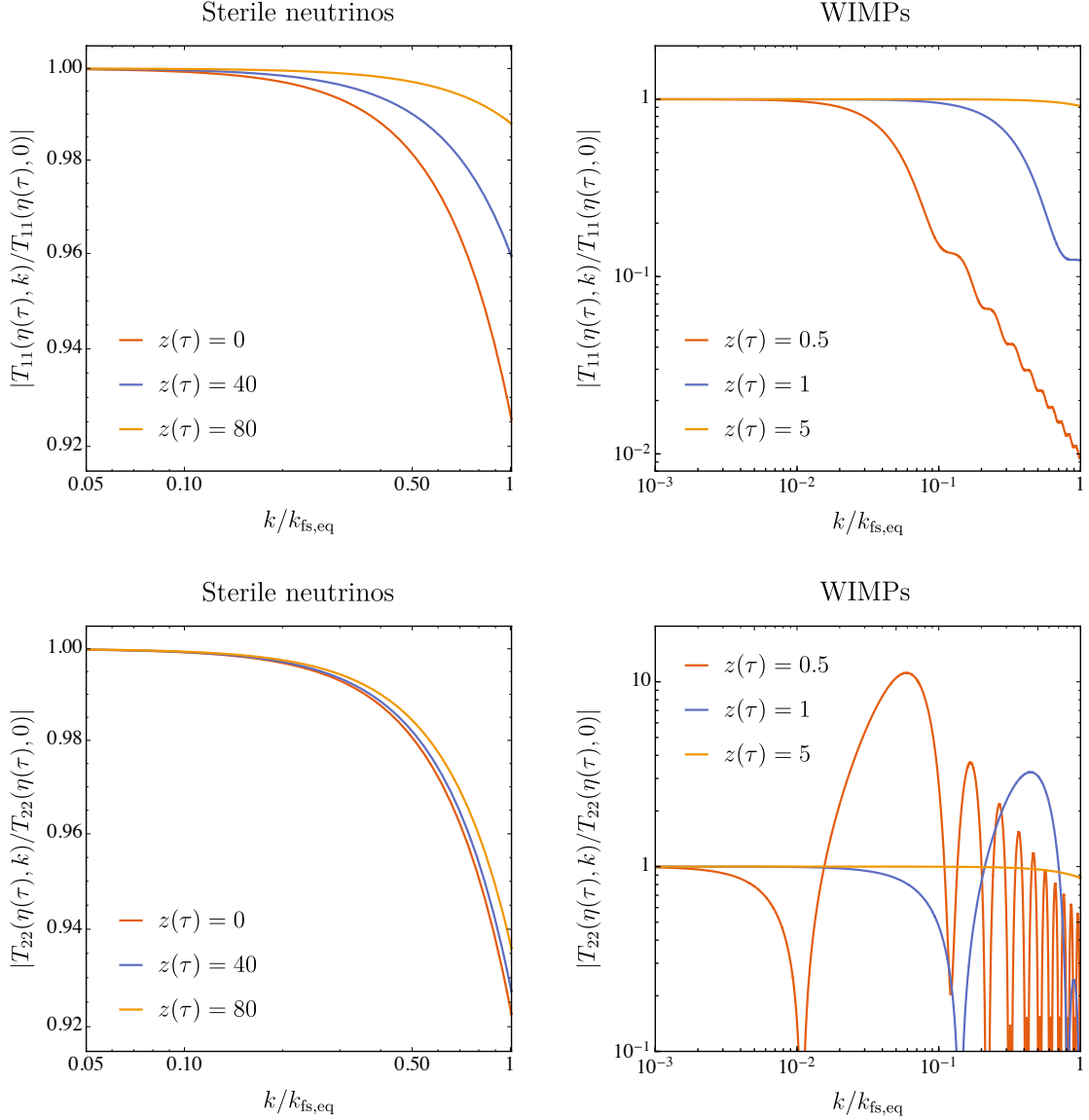


Figure 6. The normalised scalar linear transfer functions $|T_{a_s b_s}(\eta, k)/T_{a_s b_s}(\eta, 0)|$ defined through equations (3.9) and (3.10) corresponding to the growth factor $s_s^{(1)}(\eta, k)$ as a function of wave number k in units of the comoving free-streaming wave number at matter-radiation equality $k_{\text{fs,eq}}$ for sterile neutrino (left panels) and WIMP (right panels) dark matter. Shown are the density (upper panels) and velocity-divergence (lower panels) linear transfer functions for different redshifts $z(\tau)$.

corresponding to $s_v^{(n)}(\eta, k)$ for $n \in \{1, 2\}$, as a function of k in units of $k_{\text{fs,eq}}$ at three different $z(\tau)$ for both dark matter species. Because the solution corresponding to $s_v^{(2)}(\eta, k)$ has a vanishing vorticity field in the limit $k \rightarrow 0$, we display $|T_{55}^{(2)}(\eta, k)|$ without normalisation in the upper panels of figure 9. As for the scalar linear transfer functions, the qualitative behaviour of the $T_{a_v b_v}^{(n)}(\eta, k)$ in dependance of k can be read along the lines of discussion for $s_v^{(n)}(\eta, k)$ in section 3.3. The results for sterile neutrino dark matter is shown in the left panels of figures 8 and 9. The corresponding fields are damped at larger wave numbers as a consequence of

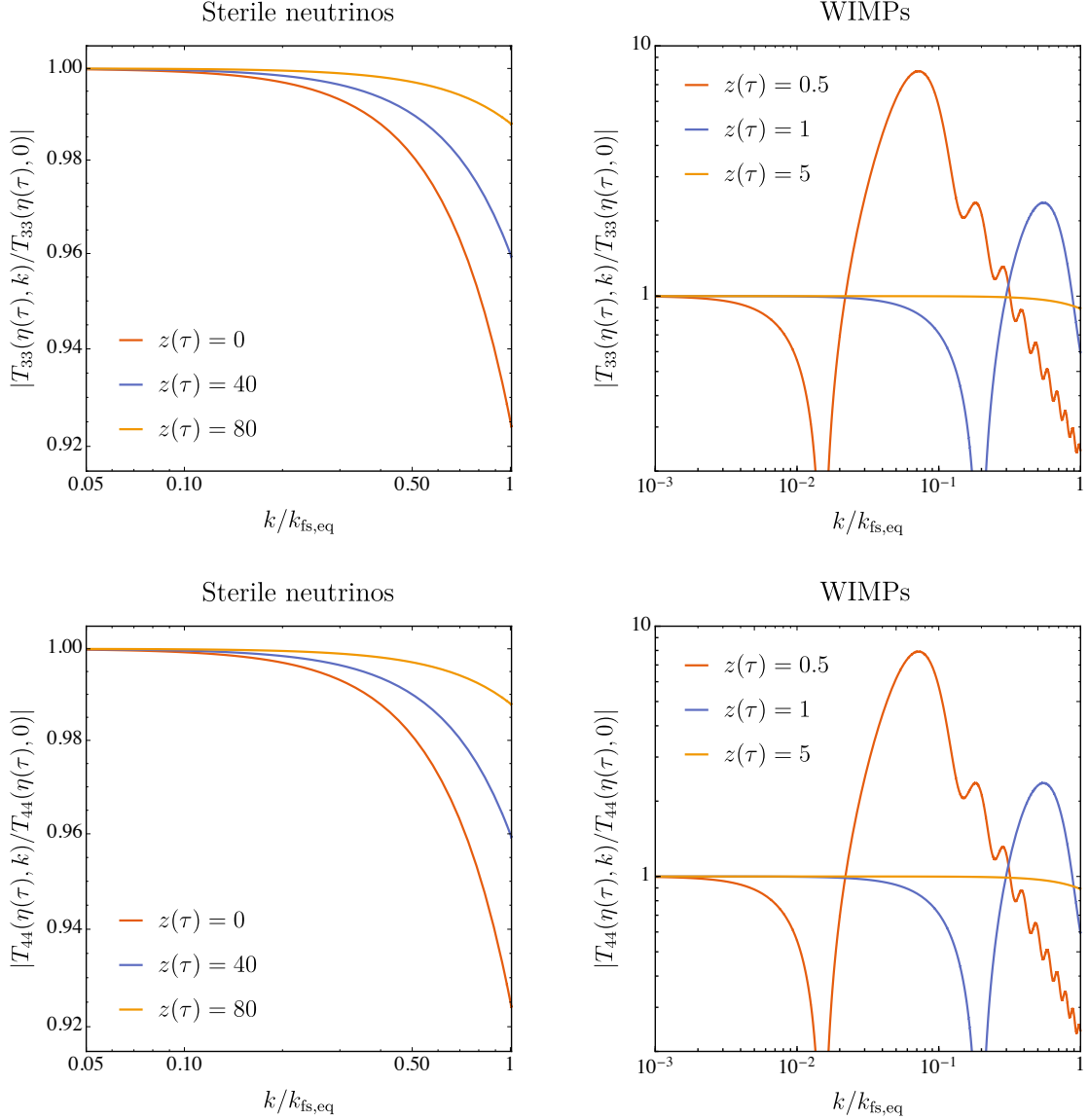


Figure 7. The normalised scalar linear transfer functions $|T_{a_s b_s}(\eta, k)/T_{a_s b_s}(\eta, 0)|$ defined through equations (3.9) and (3.10) corresponding to the growth factor $s_s^{(1)}(\eta, k)$ as a function of wave number k in units of the comoving free-streaming wave number at matter-radiation equality $k_{\text{fs,eq}}$ for sterile neutrino (left panels) and WIMP (right panels) dark matter. Shown are the isotropic (upper panels) and anisotropic (lower panels) scalar velocity dispersion linear transfer functions for different redshifts $z(\tau)$.

a negative real part of $s_v^{(n)}(\eta, k)$. Interestingly we observe less suppression for the vorticity field corresponding to $s_v^{(1)}(\eta, k)$ at late times and even an amplification of the vector velocity dispersion field at early times. The latter can be explained from the increase of $s_v^{(1)}(\eta, k)$ for larger values of $k^2 \hat{\sigma}(\eta)$ for $R(\eta) < 1/2$, corresponding to early times. The former is explained because for later times, where $R(\eta) > 1/2$, the growth factor is decreasing for larger $k^2 \hat{\sigma}(\eta)$, but $\hat{\sigma}(\eta)$ is smaller at late times than for early times for sterile neutrino dark matter. For WIMP dark matter the vector linear transfer functions are shown in the right panels of figures

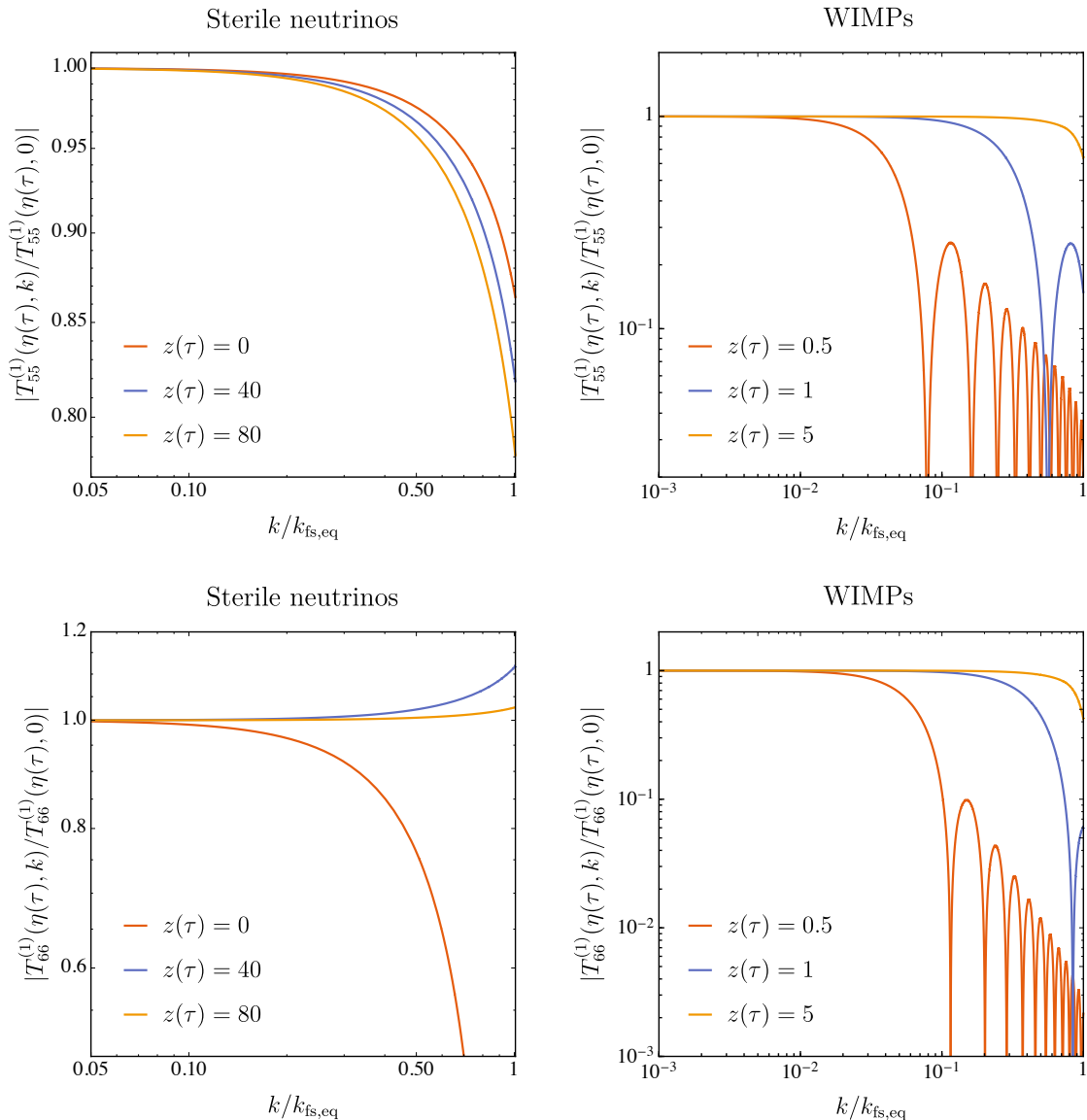


Figure 8. The normalised vector linear transfer functions $|T_{a_v b_v}^{(1)}(\eta, k)/T_{a_v b_v}^{(1)}(\eta, 0)|$ defined through equations (3.9) and (3.10) corresponding to the growth factor $s_v^{(1)}(\eta, k)$ as a function of wave number k in units of the comoving free-streaming wave number at matter-radiation equality $k_{\text{fs,eq}}$ for sterile neutrino (left panels) and WIMP (right panels) dark matter. Shown are the vorticity (upper panels) and vector velocity dispersion (lower panels) linear transfer functions for different redshifts $z(\tau)$.

8 and 9. Here $\hat{\sigma}(\eta)$ is at late times large enough to enter the regime where $s_v^{(n)}(\eta, k)$ develops an imaginary part and the corresponding fields oscillate. While the amplitude of $T_{a_v b_v}^{(n)}(\eta, k)$ is smaller than $T_{a_v b_v}^{(n)}(\eta, 0)$ for the $n = 1$ fields, the $n = 2$ fields have a strong amplification similar to the scalar case.

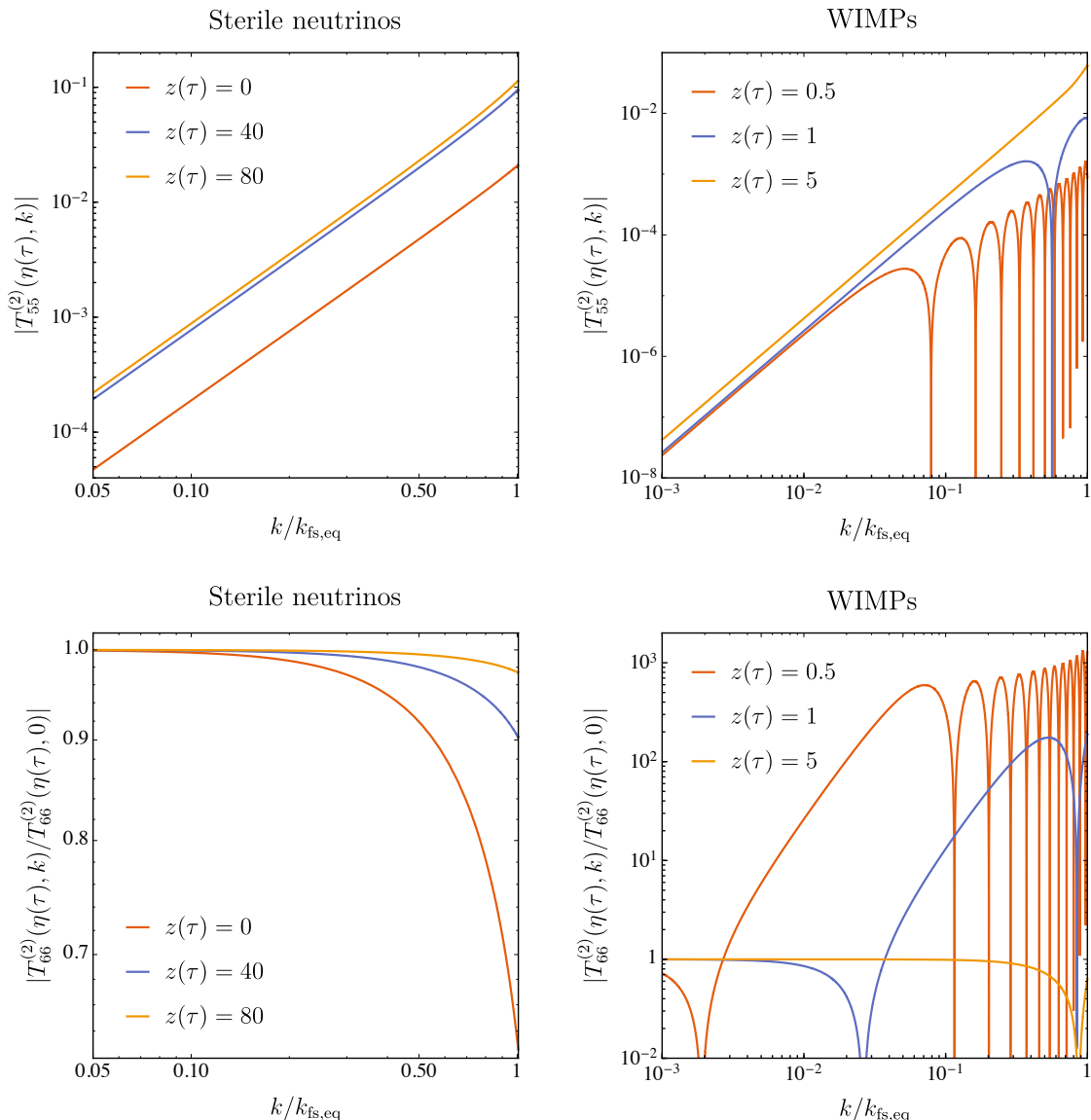


Figure 9. The (normalised) vector linear transfer functions $|T_{a_v b_v}^{(2)}(\eta, k)/T_{a_v b_v}^{(2)}(\eta, 0)|$ defined through equations (3.9) and (3.10) corresponding to the growth factor $s_v^{(2)}(\eta, k)$ as a function of wave number k in units of the comoving free-streaming wave number at matter-radiation equality $k_{\text{fs,eq}}$ for sterile neutrino (left panels) and WIMP (right panels) dark matter. Shown are the vorticity (upper panels) and vector velocity dispersion (lower panels) linear transfer functions for different redshifts $z(\tau)$.

5 Conclusion

In summary, we have studied an extension of the standard pressureless perfect fluid approximation for dark matter by taking the velocity dispersion tensor as an additional field into account. Neglecting all interaction of dark matter besides gravity, and assuming a kinetic description in terms of classical particles, we have obtained an equation of motion for the velocity dispersion tensor by taking the second cumulant of the Vlasov equation.

The set of evolution equations is closed by neglecting the third cumulant of the local

dark matter velocity distribution. In a subsequent step, we have decomposed the velocity dispersion tensor into scalar, vector and tensor fields. Together with the density and velocity fields one obtains in total four scalar fields, two solenoidal vector fields and one symmetric, transverse and traceless second-rank tensor field.

Maybe the most significant modification of the single-stream approximation based on an ideal fluid picture comes from a homogeneous and isotropic expectation value of the trace of the velocity dispersion tensor. On a technical level, the presence of such an expectation value has the consequence that it destroys the apparent self-consistency of the single-stream approximation. Perturbations in the scalar fields that parameterise the velocity dispersion tensor can now directly be generated by linear mixing or evolution from other scalar perturbations. This is important because it allows to go beyond the shell-crossing singularity and to address also late times and small scales.

Interestingly, the evolution equation for the velocity dispersion expectation value contains a back-reaction term at quadratic order in perturbations. Physically, this term describes how velocity dispersion grows again at late times (after a decrease due to the cosmological expansion at earlier times) due to large inhomogeneities in particular at small scales. Technically, this back-reaction effect is proportional to an integral over the power spectrum of scalar perturbations that is strongly dominated by the small scale or ultraviolet regime. Beyond our present approximation, there is also a similar contribution involving an integration over the power spectrum of vector perturbations. This ultraviolet sensitivity makes it particularly interesting to compare different dark matter candidates.

We concentrate here in particular on a scenario where dark matter consists of rather light sterile neutrinos of mass $m \sim 1$ keV and weakly interacting massive particles with mass in the range $m \sim 100$ GeV. The latter are much colder than the former in the sense that they have initially, at matter-radiation equality, a much smaller velocity dispersion. However, this implies that the scalar power spectrum extends much further into the ultraviolet. As we show, the non-linear back-reaction effect is then rather strong at late times, leading to a strong increase of the velocity dispersion expectation value.

In the present paper we have concentrated on a relatively simple approximation where the background is evolved non-linearly including the back-reaction effects from integrals over the power spectra of perturbations. The perturbations, or deviations from the homogeneous and isotropic background, are propagated linearly, however. While many qualitative effects can be well studied on this basis, one should keep in mind that non-linear effects in the evolution of perturbations can change the picture quantitatively, in particular at small scales and late times. Because of the ultraviolet dominance described above, this can also affect the evolution of the velocity dispersion expectation value. In future work we plan to take such effects into account. This could be done perturbatively but also using resummation schemes [13–35] and the non-perturbative renormalisation group [56, 57]. We are particularly motivated by the perspective that such a theoretical framework can go beyond the limitations of the conventional pressureless perfect fluid approximation when it comes to shell-crossing at late times and small scales. This could extend the range of applicability of semi-analytical techniques for cosmological structure formation substantially and thereby lead to an improved understanding of dark matter and late time cosmology.

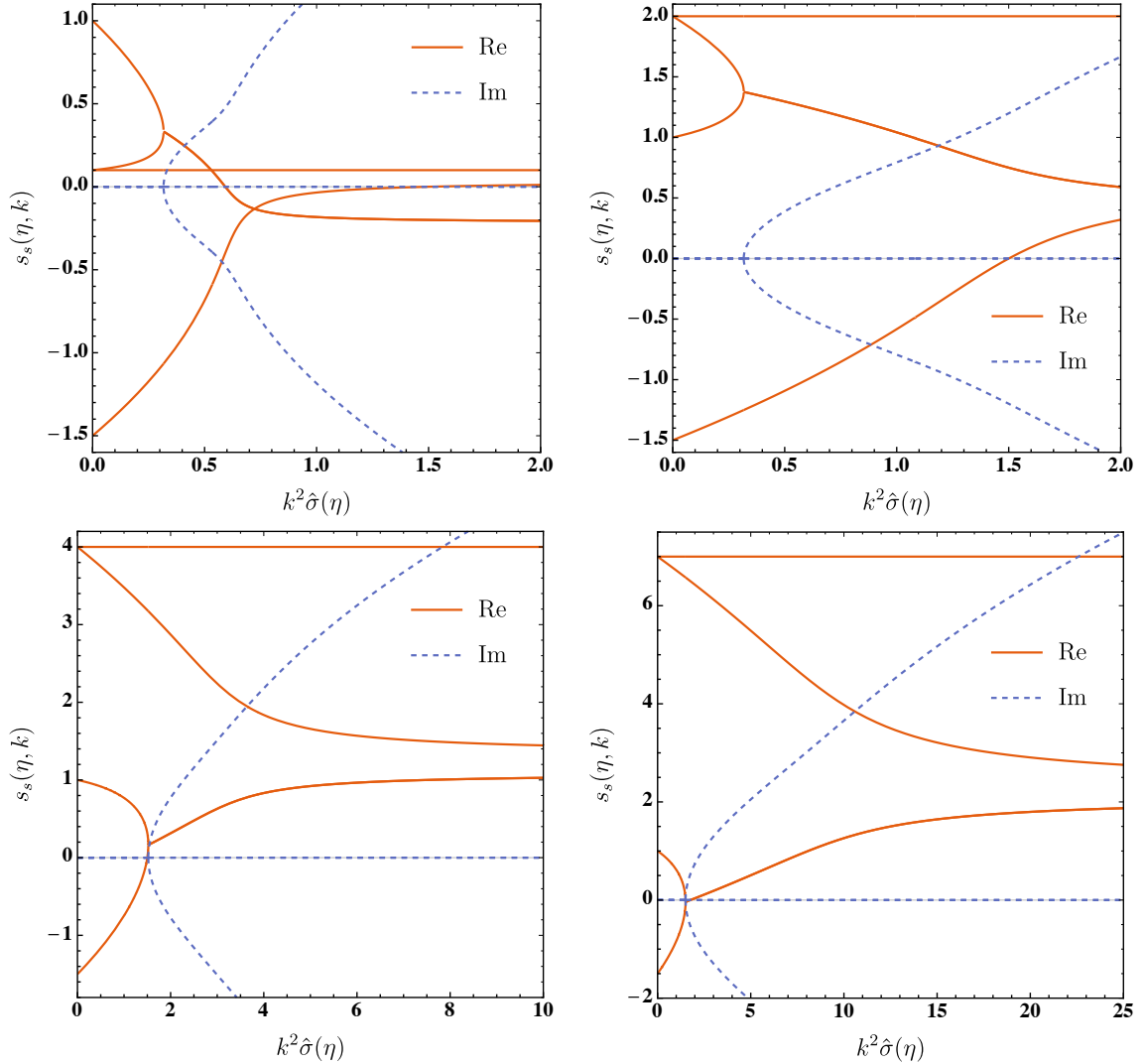


Figure 10. Growth factors $s_s^{(n)}(\eta, k)$ of the scalar fluctuation fields for $n \in \{1, 2, 3, 4\}$ as a function of the combination $k^2 \hat{\sigma}(\eta)$ for negative values of $R(\eta)$. The growth factors are displayed for $R(\eta) = -1/10$ (upper left panel), for $R(\eta) = -2$ (upper right panel), for $R(\eta) = -4$ (lower left panel) and for $R(\eta) = -7$ (lower right panel). A detailed discussion is given below.

A Growth factors of the scalar and vector fields for negative $R(\eta)$

For curiosity we extend the discussion in sections 3.2 and 3.3 and discuss the growth factors $s_s^{(n)}(\eta, k)$ for $n \in \{1, 2, 3, 4\}$ for $R(\eta) < 0$ in figure 10. In this case the scalar growth factors $s_s^{(n)}(\eta, k)$ for $n \in \{1, 3, 4\}$ are positive for small enough $k^2 \hat{\sigma}(\eta)$. As in the positive $R(\eta)$ case we only discuss $s_s^{(n)}(\eta, k)$ for $n \in \{1, 2, 3\}$ since $s_s^{(4)}(\eta, k)$ does not depend on $k^2 \hat{\sigma}(\eta)$. For $-3/4 < R(\eta) < 0$ the growth factors $s_s^{(1)}(\eta, k)$ and $s_s^{(3)}(\eta, k)$ develop an imaginary part at larger $k^2 \hat{\sigma}(\eta)$ and subsequently their coinciding real parts turn negative. The negative $s_s^{(2)}(\eta, k)$ is real and has a zero-crossing at $k^2 \hat{\sigma}(\eta) = 3/2$ and is positive for larger $k^2 \hat{\sigma}(\eta)$. This is shown in the upper left panel of figure 10 for $R(\eta) = -1/10$. The only change for $-3 < R(\eta) \leq -3/4$ is that the coinciding real parts of $s_s^{(1)}(\eta, k)$ and $s_s^{(3)}(\eta, k)$ are positive

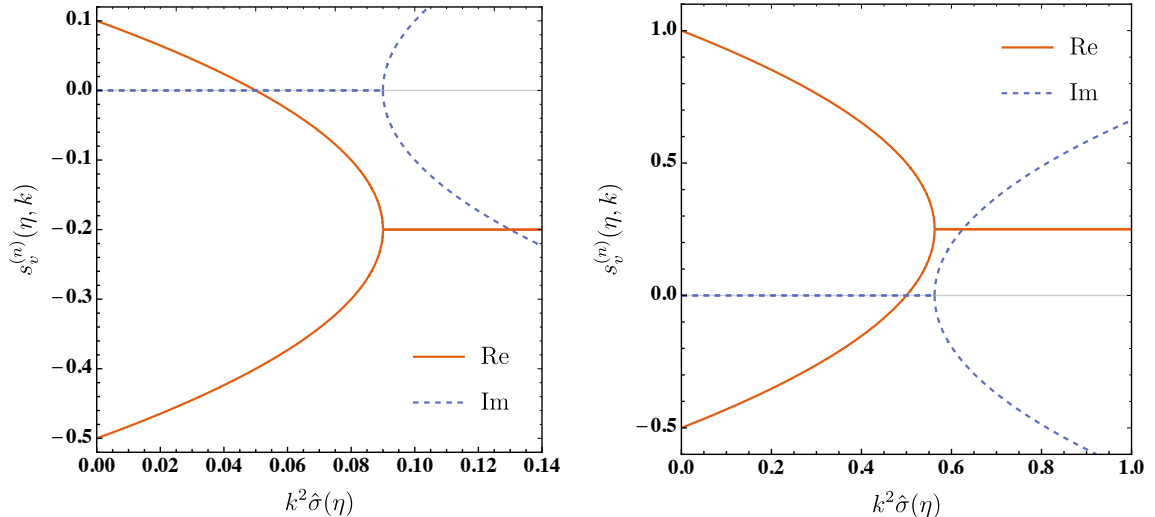


Figure 11. Growth factors $s_v^{(n)}(\eta, k)$ of the vector fluctuation fields for $n \in \{1, 2\}$ as a function of the combination $k^2 \hat{\sigma}(\eta)$ for negative values of $R(\eta)$. The left panel shows the growth factors for $R(\eta) = -1/10$ while the right panel is for $R(\eta) = -1$. A detailed discussion is given below.

for all $k^2 \hat{\sigma}(\eta)$ as shown in the upper right panel of figure 10 for $R(\eta) = -2$. In the range $-6 < R(\eta) \leq -3$ we find that $s_s^{(1)}(\eta, k)$ and $s_s^{(2)}(\eta, k)$ develop imaginary parts for larger $k^2 \hat{\sigma}(\eta)$ and their real parts coincide and are positive. The growth factors $s_s^{(1)}(\eta, k)$ and $s_s^{(2)}(\eta, k)$ are real and positive for all $k^2 \hat{\sigma}(\eta)$. This is shown in the lower left panel of figure 10 for $R(\eta) = -4$. Finally, for $-\infty < R(\eta) \leq -6$ the growth factor $s_s^{(1)}(\eta, k)$ turns negative at $k^2 \hat{\sigma}(\eta) = 3/2$, develops an imaginary part and subsequently the real part turns positive again for larger $k^2 \hat{\sigma}(\eta)$. On the other hand $s_s^{(2)}(\eta, k)$ develops a imaginary part and subsequently the real part turn positive for larger $k^2 \hat{\sigma}(\eta)$. This is shown in the lower right panel of figure 10 for $R(\eta) = -7$.

The vector growth factors $s_v^{(n)}(\eta, k)$ for $n \in \{1, 2\}$ for $R(\eta) < 0$ are displayed in figure 11. For $-1/2 < R(\eta) < 0$ the growth factor $s_v^{(2)}(\eta, k)$ is positive for small enough $k^2 \hat{\sigma}(\eta)$ and turns negative for larger $k^2 \hat{\sigma}(\eta)$. Subsequently both growth factors develop an imaginary part and the real parts are coinciding and negative. This is shown in the left panel of figure 11 for $R(\eta) = -1/10$. In the range $-\infty < R(\eta) < -1/2$ the growth factors $s_v^{(1)}(\eta, k)$ turns positive for larger $k^2 \hat{\sigma}(\eta)$ and develops an imaginary part. Subsequently $s_v^{(1)}(\eta, k)$ and $s_v^{(2)}(\eta, k)$ develop imaginary parts and their real parts coincide and are positive. This is shown in the right panel of figure 11 for $R(\eta) = -1$.

Acknowledgments

The work of S. F. is part of the DFG collaborative research centre SFB 1225 (ISOQUANT).

References

- [1] SDSS Collaboration, *The Three-Dimensional Power Spectrum of Galaxies from the Sloan Digital Sky Survey*, *Astrophys. J.* **606** (2004) 702.

- [2] 2dFGRS Team, *The 2dF Galaxy Redshift Survey: power-spectrum analysis of the final data set and cosmological implications*, *Mon. Notices Royal Astron. Soc.* **362** (2005) 505.
- [3] Y. B. Zeldovich, *Gravitational Instability: An Approximate Theory for Large Density Perturbations*, *Astron. Astrophys.* **5** (1970) 84.
- [4] F. Bernardeau, S. Colombi, E. Gaztañaga & R. Scoccimarro, *Large-scale structure of the Universe and cosmological perturbation theory*, *Phys. Rep.* **367** (2002) 1.
- [5] M. Davis, G. Efstathiou, C. S. Frenk & S. D. M. White, *The evolution of large-scale structure in a universe dominated by cold dark matter*, *Astrophys. J.* **292** (1985) 371.
- [6] V. Springel et. al., *Simulations of the formation, evolution and clustering of galaxies and quasars*, *Nature* **435** (2005) 629.
- [7] J. N. Fry, *The galaxy correlation hierarchy in perturbation theory*, *Astrophys. J.* **279** (1984) 499.
- [8] M. H. Goroff, B. Grinstein, S.-R. Rey & M. B. Wise, *Coupling of modes of cosmological mass density fluctuations*, *Astrophys. J.* **311** (1986) 6.
- [9] N. Makino, M. Sasaki & Y. Suto, *Analytic approach to the perturbative expansion of nonlinear gravitational fluctuations in cosmological density and velocity fields*, *Phys. Rev. D* **46** (1992) 585.
- [10] B. Jain & E. Breitschinger, *Second-order power spectrum and nonlinear evolution at high redshift*, *Astrophys. J.* **431** (1994) 495.
- [11] R. Scoccimarro & J. Frieman, *Loop corrections in nonlinear cosmological perturbation theory*, *Astrophys. J. Suppl. Ser.* **105** (1996) 37.
- [12] R. Scoccimarro & J. Frieman, *Loop corrections in nonlinear cosmological perturbation theory. II. Two-point statistics and self-similarity*, *Astrophys. J.* **473** (1996) 620.
- [13] P. Valageas, *A new approach to gravitational clustering: A path-integral formalism and large- N expansions*, *Astron. Astrophys.* **421** (2004) 23.
- [14] M. Crocce & R. Scoccimarro, *Renormalized cosmological perturbation theory*, *Phys. Rev. D* **73** (2006) 063519.
- [15] M. Crocce & R. Scoccimarro, *Memory of initial conditions in gravitational clustering*, *Phys. Rev. D* **73** (2006) 063520.
- [16] P. McDonald, *Dark matter clustering: A simple renormalization group approach*, *Phys. Rev. D* **75** (2007) 043514.
- [17] P. Valageas, *Large- N expansions applied to gravitational clustering*, *Astron. Astrophys.* **465** (2007) 725.
- [18] S. Matarrese & M. Pietroni, *Resumming cosmic perturbations*, *J. Cosmol. Astropart. Phys.* **06** (2007) 026.
- [19] K. Izumi & J. Soda, *Renormalized Newtonian cosmic evolution with primordial non-Gaussianity*, *Phys. Rev. D* **76** (2007) 083517.
- [20] A. Taruya & T. Hiramatsu, *A Closure Theory for Nonlinear Evolution of Cosmological Power Spectra*, *Astrophys. J.* **674** (2008) 617.
- [21] M. Crocce & R. Scoccimarro, *Nonlinear evolution of baryon acoustic oscillations*, *Phys. Rev. D* **77** (2008) 023533.
- [22] T. Matsubara, *Resumming cosmological perturbations via the Lagrangian picture: One-loop results in real space and in redshift space*, *Phys. Rev. D* **77** (2008) 063530.
- [23] P. Valageas, *Expansion schemes for gravitational clustering: computing two-point and three-point functions*, *Astron. Astrophys.* **484** (2008) 79.

- [24] F. Bernardeau & P. Valageas, *Propagators in Lagrangian space*, [Phys. Rev. D **78** \(2008\) 083503](#).
- [25] T. Matsubara, *Nonlinear perturbation theory with halo bias and redshift-space distortions via the Lagrangian picture*, [Phys. Rev. D **78** \(2008\) 083519](#).
- [26] M. Pietroni, *Flowing with time: a new approach to non-linear cosmological perturbations*, [J. Cosmol. Astropart. Phys. **10** \(2008\) 036](#).
- [27] F. Bernardeau, M. Crocce & R. Scoccimarro, *Multipoint propagators in cosmological gravitational instability*, [Phys. Rev. D **78** \(2008\) 103521](#).
- [28] A. Taruya, T. Nishimichi, S. Saito & T. Hiramatsu, *Nonlinear evolution of baryon acoustic oscillations from improved perturbation theory in real and redshift spaces*, [Phys. Rev. D **80** \(2009\) 123503](#).
- [29] F. Bernardeau, M. Crocce & E. Sefusatti, *Multipoint propagators for non-Gaussian initial conditions*, [Phys. Rev. D **82** \(2010\) 083507](#).
- [30] S. Anselmi, S. Matarrese & M. Pietroni, *Next-to-leading resummations in cosmological perturbation theory*, [J. Cosmol. Astropart. Phys. **06** \(2011\) 015](#).
- [31] F. Bernardeau, N. Van de Rijt & F. Vernizzi, *Resummed propagators in multicomponent cosmic fluids with the eikonal approximation*, [Phys. Rev. D **85** \(2012\) 063509](#).
- [32] F. Bernardeau, M. Crocce & R. Scoccimarro, *Constructing regularized cosmic propagators*, [Phys. Rev. D **85** \(2012\) 123519](#).
- [33] A. Taruya, F. Bernardeau, T. Nishimichi & S. Codis, *Direct and fast calculation of regularized cosmological power spectrum at two-loop order*, [Phys. Rev. D **86** \(2012\) 103528](#).
- [34] S. Anselmi & M. Pietroni, *Nonlinear power spectrum from resummed perturbation theory: a leap beyond the BAO scale*, [J. Cosmol. Astropart. Phys. **12** \(2012\) 013](#).
- [35] F. Bernardeau, N. Van de Rijt & F. Vernizzi, *Power spectra in the eikonal approximation with adiabatic and nonadiabatic modes*, [Phys. Rev. D **87** \(2013\) 043530](#).
- [36] D. Baumann, A. Nicolis, L. Senatore & M. Zaldarriaga, *Cosmological non-linearities as an effective fluid*, [J. Cosmol. Astropart. Phys. **07** \(2012\) 051](#).
- [37] J. J. M. Carrasco, M. P. Hertzberg & L. Senatore, *The effective field theory of cosmological large scale structures*, [J. High Energy Phys. **09** \(2012\) 082](#).
- [38] E. Pajer & M. Zaldarriaga, *On the renormalization of the effective field theory of large scale structures*, [J. Cosmol. Astropart. Phys. **08** \(2013\) 037](#).
- [39] L. Mercolli & E. Pajer, *On the velocity in the Effective Field Theory of Large Scale Structures*, [J. Cosmol. Astropart. Phys. **03** \(2014\) 006](#).
- [40] R. A. Porto, L. Senatore & M. Zaldarriaga, *The Lagrangian-space Effective Field Theory of large scale structures*, [J. Cosmol. Astropart. Phys. **05** \(2014\) 022](#).
- [41] J. J. M. Carrasco, S. Foreman, D. Green & L. Senatore, *The Effective Field Theory of Large Scale Structures at two loops*, [J. Cosmol. Astropart. Phys. **07** \(2014\) 057](#).
- [42] L. Senatore & M. Zaldarriaga, *The IR-resummed Effective Field Theory of Large Scale Structures*, [J. Cosmol. Astropart. Phys. **02** \(2015\) 013](#).
- [43] T. Baldauf, L. Mercolli, M. Mirbabayi & E. Pajer, *The bispectrum in the Effective Field Theory of Large Scale Structure*, [J. Cosmol. Astropart. Phys. **05** \(2015\) 007](#).
- [44] R. Angulo, M. Fasiello, L. Senatore & Z. Vlah, *On the statistics of biased tracers in the Effective Field Theory of Large Scale Structures*, [J. Cosmol. Astropart. Phys. **09** \(2015\) 029](#).
- [45] R. E. Angulo, S. Foreman, M. Schmittfull & L. Senatore, *The one-loop matter bispectrum in the Effective Field Theory of Large Scale Structures*, [J. Cosmol. Astropart. Phys. **10** \(2015\) 039](#).

- [46] L. Senatore, *Bias in the effective field theory of large scale structures*, [J. Cosmol. Astropart. Phys. **11** \(2015\) 007.](#)
- [47] V. Assassi, D. Baumann, E. Pajer, Y. Welling & D. van der Woude, *Effective theory of large-scale structure with primordial non-Gaussianity*, [J. Cosmol. Astropart. Phys. **11** \(2015\) 024.](#)
- [48] D. Blas, S. Floerchinger, M. Garny, N. Tetradis & A. Wiedemann, *Large scale structure from viscous dark matter*, [J. Cosmol. Astropart. Phys. **11** \(2015\) 049.](#)
- [49] T. Baldauf, L. Mercolli, & M. Zaldarriaga, *Effective field theory of large scale structure at two loops: The apparent scale dependence of the speed of sound*, [Phys. Rev. D **92** \(2015\) 123007.](#)
- [50] A. A. Abolhasani, M. Mirbabayi & E. Pajer, *Systematic renormalization of the effective theory of Large Scale Structure*, [J. Cosmol. Astropart. Phys. **05** \(2016\) 063.](#)
- [51] D. Bertolini, K. Schutz, M. P. Solon, J. R. Walsh & K. M. Zurek, *Non-Gaussian covariance of the matter power spectrum in the effective field theory of large scale structure*, [Phys. Rev. D **93** \(2016\) 123505.](#)
- [52] D. Bertolini, K. Schutz, M. P. Solon & K. M. Zurek, *The trispectrum in the Effective Field Theory of Large Scale Structure*, [J. Cosmol. Astropart. Phys. **06** \(2016\) 052.](#)
- [53] D. Bertolini & M. P. Solon, *Principal shapes and squeezed limits in the effective field theory of large scale structure*, [J. Cosmol. Astropart. Phys. **11** \(2016\) 030.](#)
- [54] E. O. Nadler, A. Perko & L. Senatore, *On the bispectra of very massive tracers in the Effective Field Theory of Large-Scale Structure*, [J. Cosmol. Astropart. Phys. **02** \(2018\) 058.](#)
- [55] G. Cusin, M. Lewandowski & F. Vernizzi, *Dark energy and modified gravity in the Effective Field Theory of Large-Scale Structure*, [J. Cosmol. Astropart. Phys. **04** \(2018\) 005.](#)
- [56] S. Matarrese & M. Pietroni, *Baryonic Acoustic Oscillations via the Renormalization Group*, [Mod. Phys. Lett. **A 23** \(2008\) 025.](#)
- [57] S. Floerchinger, M. Garny, N. Tetradis & U. A. Wiedemann, *Renormalization-group flow of the effective action of cosmological large-scale structures*, [J. Cosmol. Astropart. Phys. **01** \(2017\) 048.](#)
- [58] S. Pueblas & R. Scoccimarro, *Generation of vorticity and velocity dispersion by orbit crossing*, [Phys. Rev. D **80** \(2009\) 043504.](#)
- [59] M. Pietroni, G. Mangano, N. Saviano & M. Viel, *Coarse-grained cosmological perturbation theory*, [J. Cosmol. Astropart. Phys. **01** \(2012\) 019.](#)
- [60] A. Manzotti, M. Peloso, M. Pietroni, M. Viel & F. Villaescusa-Navarro, *A coarse grained perturbation theory for the Large Scale Structure, with cosmology and time independence in the UV*, [J. Cosmol. Astropart. Phys. **09** \(2014\) 047.](#)
- [61] M. McQuinn & M. White, *Cosmological perturbation theory in 1 + 1 dimensions*, [J. Cosmol. Astropart. Phys. **01** \(2016\) 043.](#)
- [62] A. Taruya & S. Colombi, *Post-collapse perturbation theory in 1D cosmology - beyond shell-crossing*, [Mon. Notices Royal Astron. Soc. **470** \(2017\) 4858.](#)
- [63] C. Rampf & U. Frisch, *Shell-crossing in quasi-one-dimensional flow*, [Mon. Notices Royal Astron. Soc. **471** \(2017\) 671.](#)
- [64] P. McDonald & Z. Vlah, *Large-scale structure perturbation theory without losing stream crossing*, [Phys. Rev. D **97** \(2018\) 023508.](#)
- [65] E. Pajer & D. van der Woude, *Divergence of perturbation theory in large scale structures*, [J. Cosmol. Astropart. Phys. **05** \(2018\) 039.](#)

- [66] M. Pietroni, *Structure formation beyond shell-crossing: nonperturbative expansions and late-time attractors*, *J. Cosmol. Astropart. Phys.* **06** (2018) 028.
- [67] P. McDonald, *How to generate a significant effective temperature for cold dark matter, from first principles*, *J. Cosmol. Astropart. Phys.* **04** (2011) 032.
- [68] V. F. Mukhanov, H. A. Feldman & R. H. Brandenberger, *Theory of cosmological perturbations*, *Phys. Rep.* **215** (1992) 203.
- [69] A. Friedman, *Über die Krümmung des Raumes.*, *Z. Phys.* **10** (1922) 377.
- [70] P. J. E. Peebles, *The Large-Scale Structure of the Universe*, Princeton University Press, Princeton NJ (1980).
- [71] E. Lifshitz, *On the gravitational stability of the expanding universe*, *J. Phys. (USSR)* **10** (1946) 116.
- [72] V. Silveira & I. Waga, *Decaying Λ cosmologies and power spectrum*, *Phys. Rev. D* **50** (1994) 4890.
- [73] R. Scoccimarro, S. Colombi, J. N. Fry, J. A. Frieman, E. Hivon & A. Melott, *Nonlinear evolution of the bispectrum of cosmological perturbations*, *Astrophys. J.* **496** (1998) 586.
- [74] R. Scoccimarro, *A New Angle on Gravitational Clustering*, *Ann. N. Y. Acad. Sci.* **927** (2001) 13.
- [75] D. Blas, M. Garny & T. Konstandin, *On the non-linear scale of cosmological perturbation theory*, *J. Cosmol. Astropart. Phys.* **09** (2013) 024.
- [76] D. Blas, J. Lesgourgues & T. Tram, *The Cosmic Linear Anisotropy Solving System (CLASS). Part II: Approximation schemes*, *J. Cosmol. Astropart. Phys.* **07** (2011) 034.
- [77] Planck Collaboration, *Planck 2015 results XIII. Cosmological parameters*, *Astron. Astrophys.* **594** (2016) A13.
- [78] D. J. Eisenstein & W. Hu, *Power spectra for cold dark matter and its variants*, *Astrophys. J.* **511** (1999) 5.
- [79] D. Boyanovsky, *Free streaming in mixed dark matter*, *Phys. Rev. D* **77** (2008) 023528.
- [80] D. Boyanovsky, H. J. de Vega & N. G. Sanchez, *Dark matter transfer function: Free streaming, particle statistics, and memory of gravitational clustering*, *Phys. Rev. D* **78** (2008) 063546.
- [81] D. Boyanovsky & J. Wu, *Small scale aspects of warm dark matter: Power spectra and acoustic oscillations*, *Phys. Rev. D* **83** (2011) 043524.